

Mis en forme : Surlignage

1 Supercooled liquid water clouds observed over Dome C,

2 Antarctica: temperature sensitivity and **surface radiation**

3 **impacts radiative forcing**

4

5 Philippe Ricaud¹, Massimo Del Guasta², Angelo Lupi³, Romain Roehrig¹, Eric Bazile¹,

6 Pierre Durand⁴, Jean-Luc Attié⁴, Alessia Nicosia³ and Paolo Grigioni⁵

7

8 ¹CNRM, Université de Toulouse, Météo-France, CNRS, Toulouse, France
9 (philippe.ricaud@meteo.fr; romain.roehrig@meteo.fr; eric.bazile@meteo.fr)

10 ²INO-CNR, Sesto Fiorentino, Italy (massimo.delguasta@ino.cnr.it)

11 ³ISAC-CNR, Bologna, Italy (a.lupi@isac.cnr.it; a.nicosia@isac.cnr.it)

12 ⁴Laboratoire d'Aérologie, Université de Toulouse, CNRS, UPS, Toulouse, France
13 (pierre.durand@aero.obs-mip.fr; jean-luc.attie@aero.obs-mip.fr)

14 ⁵ENEA, Roma, Italy (paolo.grigioni@enea.it)

15

16 Correspondence: philippe.ricaud@meteo.fr

17

18

19 ~~14 December 2022~~ November 2023, Version **REV01-REV02 V04+**

20

21 Submitted to **Atmospheric Chemistry and Physics**

22

23

24 **Abstract**

25 Clouds affect the Earth climate with an impact that depends on the cloud nature (solid/
26 liquid water). Although the Antarctic climate is changing rapidly, cloud observations are sparse
27 over Antarctica due to few ground stations and satellite observations. The Concordia station is
28 located on the East Antarctic Plateau (75°S, 123°E, 3233 m above mean sea level), one of the
29 driest and coldest places on Earth. We used observations of clouds, temperature, liquid water
30 and surface **radiation irradiance** performed at Concordia during 4 austral summers (December
31 2018-2021) to analyse the link between liquid water and temperature and its impact on surface

Mis en forme : Surlignage

32 **radiation irradiance** in the presence of supercooled liquid water (liquid water for temperature
33 less than 0°C) clouds (SLWCs). **Our study has shown that, at the Concordia station, the very**
34 **local structure of the ice surface highly impacts the surface albedo and therefore the radiation**
35 **budget. The ERA5 or CERES data are not able to reproduce the diurnal variation of the local**
36 **albedo. We established that a two sine empirical function with 24 h and 12 h periods well fits**
37 **the BSRN observed albedo. We show that ground based observations are likely the best way to**
38 **estimate the Net SR in Concordia.**

Mis en forme : Surlignage

39 Our analysis shows that, within SLWCs, temperature logarithmically increases from -36.0°C to -16.0°C when liquid water path increases from 1.0 to
40 14.0 g m⁻², and **The SLWC net radiative forcings positively impact the net surface radiation,**
41 **which is positive and logarithmically increases by from 0.0 to 5070.0 W m⁻² when liquid water**
42 **path increases from 1.7-2 to 3.0-5 g m⁻². This is mainly due to the longwave downward**
43 **component that logarithmically increases from 0 to 90 W m⁻² when liquid water path increases**
44 **from 1.0 to 3.5 g m⁻². The attenuation of solar incoming irradiance (that can reach more than**
45 **100 W m⁻²) is almost compensated for by the upward shortwave irradiance because of high**
46 **values of surface albedo. Based on our study, We we finally can estimate extrapolate that, over**
47 **the Antarctic continent, SLWCs have a maximum net radiative forcing rather weak over the**
48 **Eastern Antarctic Plateau (0-7 W m⁻²) but 3 to 5 times larger over Western Antarctica (0-40 W**

Mis en forme : Surlignage

Mis en forme : Surlignage
Mis en forme : Exposant, Surlignage
Mis en forme : Surlignage
Mis en forme : Exposant, Surlignage
Mis en forme : Surlignage
Mis en forme : Exposant, Surlignage
Mis en forme : Surlignage
Mis en forme : Surlignage
Mis en forme : Surlignage

49 m⁻²), maximizing in summer and over the Antarctic Peninsula. SLWCs have a great potential

Mis en forme : Surlignage

50 radiative impact over Antarctica whatever the season considered, up to 5.0 W m⁻² over the

51 Eastern Antarctic Plateau and up to 30 W m⁻² over the Antarctic Peninsula in summer.

52

53

54 **1. Introduction**

55 Antarctic clouds play an important role in the climate system by influencing the Earth's
56 radiation balance, both directly at high southern latitudes and, indirectly, at the global level
57 through complex teleconnections (Lubin et al., 1998). However, in Antarctica, ground stations
58 are mainly located on the coast and yearlong observations of clouds and associated
59 meteorological parameters are scarce. Meteorological analyses and satellite observations of
60 clouds can nevertheless give some information on cloud properties suggesting that clouds vary
61 geographically, with a fractional cloud cover ranging from about 50 to 60% around the South
62 Pole to 80-90% near the coast (Bromwich et al., 2012; Listowski et al., 2019). In situ aircraft
63 measurements performed mainly over the Western Antarctic Peninsula (Grosvenor et al., 2012;
64 Lachlan-Cope et al., 2016) and nearby coastal areas (O'Shea et al., 2017) provided new insights
65 to polar cloud modelling and highlighted sea-ice production of Cloud-Condensation Nuclei
66 (CCN) and Ice Nucleating Particles (INPs) (see e.g. Legrand et al., 2016). Mixed-phase clouds
67 (made of solid and liquid water) are preferably observed near the coast (Listowski et al., 2019)
68 with larger ice crystals and water droplets (Lachlan-Cope, 2010; Lachlan-Cope et al., 2016;
69 Grosvenor et al., 2012; O'Shea et al., 2017; Grazioli et al., 2017). Based on the raDAR/liDAR-
70 MASK (DARDAR) spaceborne products (Listowski et al., 2019), it has been found that clouds
71 are mainly constituted of ice above the continent. The abundance of Supercooled Liquid Water
72 (SLW, the water staying in liquid phase below 0°C) clouds depends on temperature and
73 liquid/ice fraction. It decreases sharply poleward, and is two to three times lower over the
74 Eastern Antarctic Plateau than over the Western Antarctic. Furthermore, the nature and optical
75 properties of the clouds depend on the type and concentration of CCN and INPs. Bromwich et
76 al. (2012) mention in their review paper that CCN and INPs are of various nature and large
77 uncertainties exist relative to their origin and abundance over Antarctica. An important point
78 remains the inability of both research and operational weather prediction models to accurately

Mis en forme : Surlignage

79 represent the clouds (especially SLW clouds, SLWCs) in Antarctica causing biases of several
80 tens W m⁻² on net surface **radiation-irradiance** (Listowski and Lachlan-Cope, 2017; King et al.,
81 2006, 2015; Bromwich et al., 2013) over and beyond the Antarctic (Lawson and Gettelman,
82 2014; Young et al. 2019). From year-long LIDAR observations of mixed-phase clouds at South
83 Pole (Lawson and Gettelman, 2014), SLWCs were shown to occur more frequently than in
84 earlier aircraft observations or weather model simulations, leading to biases in the surface
85 radiation budget estimates.

Mis en forme : Surlignage

86 Liquid water in clouds may occur in supercooled form due to a relative lack of ice nuclei
87 for temperature greater than -39°C and less than 0°C. Very little SLW is then expected because
88 the ice crystals that form in this temperature range will grow at the expense of liquid droplets
89 (called the “Wegener-Bergeron-Findeisen” process; Wegener, 1911; Bergeron, 1928;
90 Findeisen, 1938; Storelvmo and Tan, 2015). Nevertheless, SLW is often observed at negative
91 temperatures higher than -20°C at all latitudes being a danger to aircraft since icing on the wings
92 and airframe can occur, reducing lift, and increasing drag and weight. As temperature decreases
93 to -36°C, SLW dramatically lessens, so it is highly difficult 1) to observe SLWCs and 2) to
94 quantify the amount of liquid water present in SLWCs. But during the Year Of Polar Prediction
95 (YOPP) international campaign, recent observations performed at the Dome C station in

96 Antarctica of **2-two** case studies in December 2018 have revealed SLWCs with temperature
97 between -20°C and -30°C and Liquid Water Path (LWP, the liquid water content integrated
98 along the vertical) between 2 to 20 g m⁻², as well as a considerable impact on the net **sSurface**
99 **Radiation-irradiance (SR)** that exceeded the simulated values by 20-50 W m⁻² (Ricaud et al.,
100 2020).

Mis en forme : Surlignage

Mis en forme : Surlignage

101 The Dome C (Concordia) station, jointly operated by French and Italian institutions in the
102 Eastern Antarctic Plateau (75°06'S, 123°21'E, 3233 m above mean sea level, amsl), is one of
103 the driest and coldest places on Earth with surface temperatures ranging from about -20°C in

104 summer to -70°C in winter. There are three-four main instruments relevant to this study that
 105 have been routinely running for about 10 years: 1) The H₂O Antarctica Microwave
 106 Stratospheric and Tropospheric Radiometer (HAMSTRAD, Ricaud et al., 2010a) to obtain
 107 vertical profiles of temperature and water vapour, as well as the LWP. 2) The tropospheric
 108 depolarization LIDAR (Tomasi et al., 2015) to obtain vertical profiles of backscatter and
 109 depolarization to be used for the detection of SLWCs. **3) An Automated Weather Station**
 110 (**AWS**) to provide screen-level air temperature. And **34) The Baseline Surface Radiation**
 111 Network (BSRN) station to measure surface longwave (4–50 μm) and shortwave (0.3–3 μm),
 112 downward and upward surface radiation irradiance (**SRE**) from which the **Net net SRsurface**
 113 **irradiance (F_{Net})**, calculated as the difference between the downward and upward
 114 **SRscomponents**, can be computed (Driemel et al., 2018) as:

$$F_{Net} = (F_{LW}^{Down} - F_{LW}^{Up}) + (F_{SW}^{Down} - F_{SW}^{Up}) \quad (1)$$

$$\text{Net} = \text{LWD} - \text{LWU} + \text{SWD} - \text{SWU} \quad (1)$$

115 where F_{LW}^{Down} , F_{LW}^{Up} , F_{SW}^{Down} and F_{SW}^{Up} represent the longwave downward, longwave
 116 upward, shortwave downward and shortwave upward surface irradiances, respectively.
 117 LWD, LWU, SWD and SWU correspond to Longwave Downward, Longwave Upward, Shortwave
 118 Downward and Shortwave Upward SRs, respectively. At a given time, the impact of a cloud on
 119 the surface irradiance can be estimated by subtracting what would have been the cloud-free
 120 surface irradiance from the measured surface irradiance, to provide the so-called “cloud
 121 radiative forcing”. The aim of the present study is double. Using observations performed at
 122 Concordia, we intend to quantify the link between 1) temperature in the SLWCs and LWP and
 123 2) SLWC radiative forcing and LWP. Hereafter, we will use either the term “radiative flux” or
 124 “radiation”, the latter consistent with the terminology presented page 256 by Stull (1988).

125 The article is structured as follows. Section 2 presents the instruments during the period of
 126 study. In section 3, we detail the methodology employed to detect the SLWCs and calculate

Mis en forme : Surlignage

Mis en forme : Surlignage

Mis en forme : Police : Italique, Surlignage

Mis en forme : Surlignage

129 their impact on SRcloud radiative forcing, and we present the statistical method to emphasize
130 the relationship between in-cloud temperature and LWP on the one hand, and SRcloud
131 radiative forcing and LWP on the other hand. The results are highlighted in section 4 and
132 discussed in section 5, before concluding in section 6.

133

134 2. Instruments

135 We have used the observations from 34 instruments held at the Dome C station, namely
136 the LIDAR instrument to classify the cloud as SLWC, the HAMSTRAD microwave radiometer
137 to obtain LWP and vertical profile of temperature, the AWS to obtain screen-level air
138 temperature and the BSRN network to measure the SR component surface irradiances (F_{SW}^{Down} ,
139 F_{SW}^{Up} , F_{LW}^{Down} and F_{LW}^{Up}); LWD, LWU, SWD and SWU to finally to obtain F_{Net} the Net SR.

140 2.1. LIDAR

141 The tropospheric depolarization LIDAR (532 nm) has been operating at Dome C since 2008
142 (see http://lidarmax.altervista.org/englidar/_Antarctic%20LIDAR.php). The LIDAR provides
143 5-min tropospheric profiles of clouds characteristics continuously, from 20 to 7000 m above
144 ground level (agl), with a resolution of 7.5 m. For the present study, the most relevant parameter
145 is the LIDAR depolarization ratio (Mishchenko et al., 2000) that is a robust indicator of non-
146 spherical shape for randomly oriented cloud particles. A depolarization ratio below 10% is
147 characteristic of SLWC, while higher values are produced by ice particles. The possible
148 ambiguity between SLW droplets and oriented ice plates is avoided at Dome C by operating
149 the LIDAR 4° off-zenith (Hogan and Illingworth, 2003).

150 2.2. HAMSTRAD

151 HAMSTRAD is a microwave radiometer that profiles water vapour, liquid water and
152 tropospheric temperature above Dome C. Measuring at both 60 GHz (oxygen molecule line
153 (O_2) to deduce the temperature) and 183 GHz (H_2O line), this unique, state-of-the-art

Mis en forme : Surlignage

154 radiometer was installed on site for the first time in January 2009 (Ricaud et al., 2010a and b).
155 The measurements of the HAMSTRAD radiometer allow the retrieval of the vertical profiles
156 of water vapour and temperature from the ground to 10-km altitude with vertical resolutions of
157 30 to 50 m in the Planetary Boundary Layer (PBL), 100 m in the lower free troposphere and
158 500 m in the upper troposphere-lower stratosphere. **The integral along the vertical of the water**
159 **vapour concentration gives the integrated water vapour (IWV).** The time resolution is adjustable
160 and fixed at 60 seconds since 2018. Note that an automated internal calibration is performed
161 every 12 atmospheric observations and lasts about 4 minutes. Consequently, the atmospheric
162 time sampling is 60 seconds for a sequence of 12 profiles and a new sequence starts 4 minutes
163 after the end of the previous one. The temporal resolution on the instrument allows for detection
164 and analysis of atmospheric processes such as the diurnal evolution of the PBL (Ricaud et al.,
165 2012) and the presence of clouds and diamond dust (Ricaud et al., 2017) together with SLWCs
166 (Ricaud et al., 2020). In addition, the LWP (g m^{-2}) that gives the amount of liquid water
167 integrated along the vertical can also be estimated. Observations of LWP have been performed
168 when the instrument was installed at the Pic du Midi station (2877 amsl, France) during the
169 calibration/validation period in 2008 prior to its set up in Antarctica in 2009 (Ricaud et al.,
170 2010a) and during the Year Of Polar Prediction (YOPP) campaign in summer 2018-2019
171 (Ricaud et al., 2020). At the present time, it has not yet been possible to compare HAMSTRAD
172 LWP retrievals with observations from other instruments, neither at the Pic du Midi nor at
173 Dome C stations. To better evaluate its performance, the 2021-2022 and the future 2022-2023
174 summer campaigns are dedicated to in-situ observations of SLWCs. Comparisons with
175 numerical weather prediction models were showing consistent amounts of LWP at Dome C
176 when the partition function between ice and liquid water was favouring SLW for temperatures
177 less than 0°C (Ricaud et al., 2020). Note that microwave observations at 60 and 183 GHz are
178 not sensitive to ice crystals. This has already been discussed in Ricaud et al. (2017) when

Mis en forme : Surlignage

179 considering the study of diamond dust in Antarctica. As a consequence, possible precipitation
180 of ice, within or below SLW clouds, as detected by the LIDAR, does not affect the retrievals
181 of temperature, water vapour and liquid water.

Mis en forme : Surlignage

182 2.3. AWS

Mis en forme : Surlignage

183 An American Automated Weather Station (AWS) is installed at Concordia about 500 m
184 away from the station and can provide screen-level air temperature (T_a) every 10 minutes. Data
185 are freely available at <https://amrc.ssec.wisc.edu/data/archiveaws.html>.

Mis en forme : Surlignage

Mis en forme : Surlignage

Mis en forme : Anglais (Royaume-Uni)

186 2.4. BSRN

Mis en forme : Surlignage

187 The BSRN sensors at Dome C are mounted at the Astroconcordia/Albedo-Rack sites, with
188 upward and downward looking, heated and ventilated Kipp&Zonen CM22 pyranometers and
189 CG4 pyrgeometers providing measurements of hemispheric downward and upward broadband
190 shortwave (SW, 0.3–3 μm) and longwave (LW, 4–50 μm) horizontal radiative fluxes irradiances
191 at the surface, respectively. These data are used to retrieve values of net surface
192 radiation irradiances. All these measurements follow the rules of acquisition, quality check and
193 quality control of the BSRN (Driemel et al., 2018).

Mis en forme : Surlignage

Mis en forme : Surlignage

194 2.4.1. Period of study

Mis en forme : Surlignage

195 From the climatological study presented in Ricaud et al. (2020), the SLWCs are mainly
196 observed above Dome C in summer, with a higher occurrence in December than in January:
197 26% in December against 19% in January representing the percentage of days per month that
198 SLW clouds were detected during the YOPP campaign (summer 2018-2019) within the LIDAR
199 data for more than 12 hours per day. We have thus concentrated our analysis on December and
200 the 4 years: 2018-2021. Since we have to use the three four data sets (LIDAR, HAMSTRAD,
201 AWS and BSRN) in time coincidence, the actual number of days per year and the time sampling
202 for each day selected in our analysis is presentedare detailed in Table 1.

Mis en forme : Surlignage

204

205 3. Methodology

206 3.1. SLWC detection and Surface Radiation Impact

207 Consistent with Ricaud et al. (2020), we use LIDAR observations to discriminate between
208 SLW and ice in a cloud. High values of LIDAR backscatter coefficient ($\beta > 100 \beta_{\text{mol}}$, with β_{mol}
209 the molecular backscatter) associated with very low depolarization ratio (<-5%) signifies the
210 presence of an SLWC whilst high depolarization ratio (>20%) indicates the presence of an ice
211 cloud or precipitation. Once the SLWC is detected both in time and altitude, the ~~regular~~
212 temperature (~~OT~~) profile within the cloud and the LWP measured by the HAMSTRAD
213 radiometer in time coincidence are selected together with the surface irradiances~~SR~~ observed
214 by the BSRN instruments~~-Net, LWD, LWU, SWD and SWU SR~~.

The LIDAR profiles are interpolated along the temperature vertical grid and then according to the temperature time sampling. As a consequence, for a given time and height, we have a depolarization ratio, a backscatter signal value, a regular temperature and as well as a (not height-dependent) IWP and LWP values. The same method is used for FSR. BSRN FSRs are time interpolated to be coincident with the LWP values other parameters. So, for a given time, we have a set of BSRN FSRs (F_{IW}^{Down} , F_{IW}^{Up} , F_{SW}^{Down} , F_{SW}^{Up} , and F_{Net} , Net, LWU, LWD, SWU and SWD) and an LWP. At a (time, height) point showing high backscatter signal and low depolarization, the associated parameters (regular temperature, LWP and FSRs) are flagged as “SLW cloud”. The statistic is thus done using all the SLW-flagged points without any averaging. The temperature corresponds to the in-cloud temperature.

Figure 1 shows, as a typical example, the time evolution of the LIDAR backscatter coefficient and depolarization ratio, as well as the HAMSTRAD LWP and temperature vertical profile for the 27 December 2021. Associated with the SLWCs, the LWP values are between 1.0 and increases with time from 1.0 to 3.0 g m^{-2} . The SLWCs are present over a temperature

range varying from about -28.0 °C to -33.0 °C. Note the cloud present at 04:00-05:00 UTC that is not labelled as a SLWC but rather as an ice cloud (high backscatter and high depolarization signals) with no associated increase of LWP and temperature above -28.0 °C.

Figure 2 highlights the time evolution of the SLWC obtained on 27 December 2021 together with some snapshots from the HALO-CAM video camera taken with or without SLWC on: 01:00 (no SLWC), 07:19 (SLWC), 09:00 (no SLWC), 10:14 (SLWC), 13:00 (no SLWC), 16:03 (SLWC), 18:01 (no SLWC) and 20:53 UTC (SLWC). SLWCs (high backscatter and low depolarization signals) are clearly detected at 07:00-08:00, 10:00-11:00, 16:00-17:00, 21:00-22:00 and 23:00-24:00 UTC over an altitude range 500-1000 m above ground level (agl). In general, SLWCs observed over the station did not correspond to overcast conditions.

3.2. Cloud Radiative Forcing

The cloud radiative forcing (ΔF) can be defined as:

$$\Delta F = F - FCF \quad (2)$$

242 for the net, longwave downward, longwave upward, shortwave downward and shortwave
 243 upward surface irradiances, with FCF being the surface irradiance in cloud-free conditions. One
 244 of the main difficulties in computing ΔF is to estimate FCF . Several studies have been
 245 performed (reference irradiances measured over one day when clouds are absent, radiative
 246 transfer calculations) but the most robust method has been to use a parameterization of the
 247 downward longwave and shortwave surface irradiances widely used in the community. In
 248 Dutton et al. (2004), cloud-free downward shortwave surface irradiance (FCF_{SW}^{Down}) is
 249 parameterized as:

$$FCF_{SW}^{Down} = a \cos(z)^b c^{\left(\frac{1}{\cos(z)}\right)} \quad (3)$$

where z is the solar-zenith angle, and a , b , and c are coefficients optimized using well-identified cloud-free situations. In Dupont et al. (2008), cloud-free downward longwave surface irradiance (FCF_W^{Down}) is parameterized as:

Mis en forme : Surlignage

Mis en forme : Police : Italique, Surlignage

Mis en forme : Surlignage

Mis en forme : Retrait : Première ligne : 0,75 cm, Interligne : Double

Mis en forme : Interligne : Double

Mis en forme : Surlignage

Mis en forme : Interligne : Double

Mis en forme : Surlignage

254
$$FCF_{SW}^{Down} = \varepsilon_{sw} \sigma T_{sw}^4 \quad (4)$$

255 where T_{sw} is the screen-level air temperature in Kelvin (K), σ the Stephan-Boltzmann's constant*
 256 and ε_{sw} the apparent atmospheric emissivity. The latter is supposed to be a function of the
 257 integrated water vapor (IWV) following the equation:

258
$$\varepsilon_{sw} = 1 - (1 + IWV) \exp(-(d + e \times IWV)^f) \quad (5)$$

259 where d , e and f are coefficients that need to be optimized using cloud-free situations. The
 260 cloud-free upward shortwave surface irradiance (FCF_{SW}^{Up}) is evaluated from FCF_{SW}^{Down} with the
 261 surface albedo ($A_{BSRN} = F_{SW}^{Up}(BSRN)/F_{SW}^{Down}(BSRN)$) calculated from observations:

262
$$FCF_{SW}^{Up} = A_{BSRN} \times FCF_{SW}^{Down} \quad (6)$$

263 where $F_{SW}^{Up}(BSRN)$ and $F_{SW}^{Down}(BSRN)$ are the upward and downward shortwave surface
 264 irradiance measured by the BSRN instruments, respectively. With this method, we take into
 265 account the actual shape of the surface, and in particular its rough structure caused by the
 266 sastrugi (see section 5.5). Thus, the surface albedo varies with the sun angles (azimuthal and
 267 zenithal) and cannot be considered as constant over the diurnal cycle. Note that computationally
 268 simple, theoretically based parameterization for the broadband albedo of snow and ice can
 269 accurately reproduce the theoretical broadband albedo under a wide range of snow, ice, and
 270 atmospheric conditions (Gardner and Sharp, 2010).

271 The cloud-free upward longwave radiation (FCF_{LW}^{Up}) is evaluated as:

272
$$FCF_{LW}^{Up} = \varepsilon_{sw} \sigma T_{sw}^4 + (1 - \varepsilon_{sw}) FCF_{LW}^{Down} \quad (7)$$

273 where T_{sw} is the surface temperature and the surface emissivity ε_{sw} is assumed constant and equal
 274 to 0.99. Screen-level temperatures T_{sw} are provided by the American automated weather station
 275 (AWS) situated at ~500 m from the Concordia base. T_{sw} is diagnosed based on equation (7) by
 276 using the BRSN upward and downward longwave surface irradiances. IWV is provided by the
 277 HAMSTRAD measurements.

Mis en forme

[1]

Mis en forme : Surlignage

Mis en forme : Interligne : Double

Mis en forme

[2]

Mis en forme

[3]

Mis en forme

[4]

Mis en forme : Interligne : Double

Mis en forme

[5]

Mis en forme

[6]

Mis en forme

[7]

Mis en forme

[8]

Mis en forme : Interligne : Double

Mis en forme

[9]

Mis en forme

[10]

Mis en forme : Surlignage

Mis en forme : Retrait : Première ligne : 0,75 cm, Interligne : Double

Mis en forme

[11]

Mis en forme

[12]

Mis en forme : Interligne : Double

Mis en forme : Surlignage

[13]

Mis en forme

[14]

Mis en forme

[15]

Mis en forme

[16]

Cloud-free situations are detected based on visual inspection of the LIDAR (depolarization) measurements. Depolarization ratios greater than about 1% are attributed to the presence of cloud (cirrus, mixed-phase, SLW), diamond dust, fog, etc. Thus, within each 24-hour slot covering the Decembers 2018-2021, the 1-hour periods when the depolarization ratios are less than 1% are considered as cloud-free periods. Consequently, to evaluate the surface cloud-free irradiances over the month of December and the years 2018-2021, we need to have coincident observations from the 4 BSRN instruments, the LIDAR (depolarization), HAMSTRAD and the AWS (see Table 1).

Once cloud-free situations are identified, the parametric coefficients $a-f$ are estimated minimizing a least-square cost function using the trust region reflective method (e.g., Branch et al., 1999). To assess the robustness of the estimated coefficient values, a K-fold cross-validation is performed. The learning dataset is split into 10 subsamples of equal size. 9 of them are selected to optimize the coefficient and the validation is conducted on the remaining subsample. The exercise is performed 10 times. The results are summarized below. Note that following Dupont et al. (2008), f is assumed to be equal to 1.0, and therefore not optimized.

For downward shortwave surface irradiance, the K-fold cross-validation provides the following K-fold average value (K-fold minimum and maximum are indicated within brackets):
 $a = 1360.7 [1360.5, 1360.8] \text{ W m}^{-2}$; $b = 0.990 [0.989, 0.991]$; $c = 0.964 [0.964, 0.965]$ giving a bias of $-0.002 [-0.317, 0.251] \text{ W m}^{-2}$ and a RMSE of $14.9 [10.8, 16.5] \text{ W m}^{-2}$. Similarly, for downward longwave surface irradiance, the K-fold cross-validation provides the following results: $d = 0.723 [0.722, 0.724]$; $e = 3.58 [3.57, 3.59] \text{ kg}^{-1} \text{ m}^2$; $f = 1.0$ giving a bias of $0.34 [-0.005, 0.87] \text{ W m}^{-2}$ and a RMSE of $9.26 [8.92, 9.58] \text{ W m}^{-2}$. These coefficient values are then used to compute cloud-free surface irradiances at a 1-min time resolution.

Figure 3 shows the time evolution of the cloud radiative forcing (ΔF_{net} , ΔF_{LW}^{Down} , ΔF_{LW}^{Up} , ΔF_{SW}^{Down} and ΔF_{SW}^{Up}) calculated for 27 December 2021 when SLWCs are present (see Figures 1

Mis en forme : Retrait : Première ligne : 0,75 cm, Interligne : Double

303 and 2). Over the 4 summers (December 2018–2021), we have selected 3 datasets in time
 304 coincidence with SLWC: LWP, θ and SR. In order to estimate the impact of the SLWC onto
 305 the SR, we calculated the anomaly of the daily SR with respect to the clear-sky SR associated
 306 to the same day. Since it is impossible to measure for the same day the SR with and without
 307 cloud, we have in priority looked for clear-sky days over the months of December in the 2018–
 308 2021 period. Only 5 clear-sky days were selected on: 2 and 19 December 2018, and 3, 17 and
 309 26 December 2021. These 5 days, considered as the reference SRs (SR_{ref}), are presented in
 310 Figure 3. We have also calculated (Figure 4) the time evolution of the clear-sky surface
 311 radiation variability (δSR_{ref}), namely the difference in SR observed by the BSRN instruments
 312 between each of 5 clear-sky day and the corresponding values averaged over the 5 days, for
 313 Net, LWD, LWU, SWD and SWU SR. The SR_{ref} for the 5 days shown Figure 3 are all
 314 consistent to each other with an obvious diurnal cycle in Net, LWD, LWU, SWD and SWU SR
 315 (we recall that in December there is a 24-h solar illumination at Dome C). The variability within
 316 the 5 days (δSR_{ref}) shown Figure 4 is within $\pm 20 \text{ W m}^{-2}$ for the Net SR with a greater Net SR
 317 in 2018 than in 2021, within $\pm 35 \text{ W m}^{-2}$ for LWD and LWU SR (maxima on 17 December 2021
 318 and minima on 2 December 2018), and within $\pm 25 \text{ W m}^{-2}$ for SWD and SWU SR (maxima on
 319 26 December 2021 and minima on 2 December 2018).

320 Based on these 5 SR_{ref} , we performed a systematic study over the 4 summer period by
 321 calculating the surface radiation anomaly ΔSR defined as:

$$\Delta SR = SR - SR_{ref} \quad (2)$$

322 for Net, LWD, LWU, SWD and SWU. As an example, we show in Figure 5 the time
 323 evolution for 27 December 2021 of the presence of the SLWC together with ΔSR calculated
 324 with respect to SR_{ref} set to 26 December 2021. Associated with the SLWCs, on the one hand,
 325 ΔF_{LW}^{Down} LWD and LWU ΔSR increases by to values of +30–50 and 10–30–40–90 W m^{-2} , whilst
 326 the impact on ΔF_{LW}^{Up} is negligible ($\pm 2 \text{ W m}^{-2}$). On the other hand, respectively, whilst

Mis en forme : Surlignage
 Mis en forme : Surlignage

328 ΔF_{SW}^{Down} SWD and ΔF_{SW}^{Up} SWU both similarly ΔASR decrease by $5080-150 \text{ W m}^{-2}$, respectively.
 329 The effect on ΔF_{Net} , the Net ΔASR is obviously positive ($10-100.80 \text{ W m}^{-2}$) at 07:00-08:00, 10:00-
 330 11:00, 16:00-17:00 UTC and with some weak negative values (from from -300 to -100 W m^{-2})
 331 at 21:00-22:00 and 23:00-24:00 UTC when SWLCs just appear or disappear and can possibly
 332 come from the inhomogeneity of the cloud distribution. Spikes can be attributed to cloud edge
 333 effects, when direct fraction of the solar incident radiation and an additional diffuse contribution
 334 scattered from cloud edges falls on the radiation sensor.

335 Note that spikes appear in Net ΔSR , SWU ΔSR and SWD ΔSR mainly during scattered
336 conditions and when large cloud episodes appear or disappear. They are real and can possibly
337 come from the inhomogeneity of the cloud distribution. We thus now want to statistically
338 analyse all the ΔSRF calculated in December 2018-2021 with the S_{REF} in order to assess the
339 SLWC radiative forcing as a function of LWP and to investigate the sensitivity of the
340 temperature inside the SLWCs as a function of LWP check whether the net effect of the SLWC
341 on the SR is positive or negative and to evaluate its sensitivity to liquid water amounts.

342 3.23. Statistical Method

The datasets corresponding to SLWCs periods are binned into 1°C-wide bins for in-cloud temperature θT , 0.2 g m⁻²-wide bins for LWP, and 5 W m⁻²-wide bins for ΔFSR . The number of points per bin is calculated for all the paired datasets, namely θT -LWP, and ΔSRF -LWP (ΔF_{net} -Net ASR-LWP, ΔF_{lw}^{Down} -LWD ASR-LWP, LWP-ASRF_{Up}-LWP, ΔF_{sw}^{Down} -SWD ASR-LWP and ΔF_{sw}^{Up} -SWU ASR-LWP). The 2D probability density (PD) is calculated for the paired datasets and defined as $PD_{ij} = 100 \frac{N_{ij}}{N_t}$, where N_{ij} and N_t are the count number in the bin ij and the total count number ($N_t = \sum_{j=1}^N \sum_{i=1}^M N_{ij}$), respectively, with M and N being the total number of bins in LWP on one side, and in temperature or ΔFSR on the other side, respectively. This study is focused on the evaluation of the LWP sensitivity for a given temperature and for

352 a given radiation component (Net, LWD, LWU, SWD, SWU). So, for each value of θT_j (within
 353 a 1°C -wide bin j) or ΔSRF_j (within a 5 W m^{-2} -wide bin j), a weighted average of LWP (\overline{LWP}_j)
 354 is calculated together with its associated weighted standard deviation (σ_{LWP_j}), considering all
 355 the LWP_{ij} values (within 0.2 g m^{-2} -wide bins) from $i=1$ to M , with M the total number of LWP
 356 bins and w_{ij} the weight, namely the number of points ($w_{ij} = N_{ij}$), associated to the bin ij :

$$\overline{LWP}_j = \frac{\sum_{i=1}^M w_{ij} LWP_{ij}}{\sum_{i=1}^M w_{ij}} \quad (38)$$

358 and

$$\sigma_{LWP_j} = \sqrt{\frac{\sum_{i=1}^M w_{ij} (LWP_{ij} - \overline{LWP}_j)^2}{\sum_{i=1}^M w_{ij}}} \quad (49)$$

360 For each θT and ΔSRF dataset, the distribution of the total count numbers N_{tj} per 1°C or
 361 5 W m^{-2} -wide bin ($N_{tj} = \sum_{i=1}^M N_{ij}$ with $j = 1, \dots, N$) can be fitted by a function $N(x)$, with $x =$

362 θT or ΔSRF , based on 2 to 3 Gaussian distributions as:

$$N(x) = \sum_{k=1}^{2 \text{ or } 3} a_k \exp\left(-\frac{1}{2} \left(\frac{x-\mu_k}{\sigma_k}\right)^2\right) + c_0 e \quad (50)$$

364 with a_k , μ_k and σ_k being the amplitude, the mean and the standard deviation of the k^{th} Gaussian
 365 function ($k = 1, 2$ or 3) and $c_0 e$ is a constant. We have used $k = 0, 2$ or 3 Gaussians for ΔSRF
 366 components and $k = 3$ Gaussians for θT . ("0" means that no Gaussian fit was meaningful).
 367 Table 2 lists all the fitted parameters (a_k , μ_k , σ_k and $c_0 e$ with $k = 0$ to 2 or 3).

368 In the relationship between x (θT or ΔSRF) and LWP, we have considered x_j (θT_j or
 369 ΔSRF_j) to be significant when:

$$|x_j - \mu_k| \leq \sigma_k \text{ for } k = 1 - 2 \text{ or } 3 \text{ (for } \Delta SRF \text{) or } 1 - 3 \text{ (for } \theta T \text{)} \quad (61)$$

370 and used for this significant point its average value and standard deviation, \overline{LWP}_j and σ_{LWP_j} ,
 371 respectively, with $j = 1, \dots, N$.

373 Finally, a logarithmic function of the form

Mis en forme : Surlignage

$$x = \alpha + \beta \ln(LWP) \quad (712)$$

375 has been fitted onto these significant points- where the retrieved constants α_a and β_b are shown
 376 in Table 3 for x being θT , ΔF_{net} , ΔF_{IW}^{Down} , ΔF_{IW}^{Up} , ΔF_{SW}^{Down} and ΔF_{SW}^{Up} , Net ASR, LWD ASR, LWU
 377 ASR, SWD ASR and SWU ASR.

379 4. Results

380 4.1. Temperature-Liquid Water Relationship in ~~Supercooled Liquid Water Clouds~~SLWCs

The relationship between temperature and LWP within SLWCs over the 4-summer period at Dome C is presented Figure 6.4 left in the form of a Probability Density (PD) – that is the fraction of points within each bin of 0.2 g m^{-2} width in LWP and 1.0°C width in temperature. It clearly shows a net tendency for liquid water to increase with temperature, up to $\sim 14 \text{ g m}^{-2}$ in LWP and -18°C in temperature, with two zones having a density as high as $\sim 2\%$, at $[0.5 \text{ g m}^{-2}, -33^\circ\text{C}]$ and $[1.5 \text{ g m}^{-2}, -32^\circ\text{C}]$. We have performed a weighted average of the LWPs within each temperature bin (Figure 6.4 centre). Then, we have fitted 3 Gaussian distributions to the count numbers as a function of temperature (Figure 6.4 right). If we now only consider temperature bins within one-sigma of the centre of the Gaussian distributions, we can fit the following logarithmic relation of the temperature T as a function of LWP within the SLWC (Figure 6.4 centre):

$$\theta T(LWP) = -33.8 (\pm 1.5) + 6.5 \ln(LWP) \quad (813)$$

393 for θL \in $[-36; -16]$ °C and $LWP \in [1.0; 14.0]$ g m $^{-2}$, where (± 1.5 °C) corresponds to the
 394 range where the relationship is valid within the 2 blue dashed lines in Figure 64 centre. In other
 395 words, based on our study, we have a clear evidence that supercooled liquid water content
 396 exponentially increases with temperature. Considering the temperature vs. LWP relationship,
 397 the two main Gaussian distributions are centered around -28°C and -30°C,
 398 corresponding to temperatures usually encountered in Concordia whilst the third one, far much

399 less intense, is ~~centred~~centered around -18°C, probably the signature of very unusual events
 400 occurring in Concordia as the warm-moist events. Episodes of warm-moist intrusions exist
 401 above Concordia originated from mid-latitudes (Ricaud et al., 2017 and 2020) and are known
 402 as “atmospheric rivers” (Wille et al., 2019). Although they are infrequent, they can provide high
 403 values of temperature and LWP.

404 4.2. *Radiative Forcing-Liquid Water Relationship in SLWC conditions* *Impacts of Supercooled*
 405 *Liquid Water Clouds on Surface Radiation*

406 Although the amount of LWP is very low ($\ll 20 \text{ g m}^{-2}$) at Dome C compared to what can
 407 be measured and modelled (Lemus et al., 1997) in the Arctic ($50\text{-}75 \text{ g m}^{-2}$) and at
 408 middle/tropical latitudes ($100\text{-}150 \text{ g m}^{-2}$), we intended to estimate its impact on the ~~SR~~cloud
 409 ~~radiative forcing~~ at Dome C. In Figures 7-5 to 99, the left panel presents the PDs ~~(for bins of~~
 410 0.2 g m^{-2} width in LWP and 5 W m^{-2} width in ΔSR) of the ~~surface radiation anomaly~~cloud
 411 ~~radiative forcing~~ ΔSRF as a function of the LWP, for ΔF_{net} , ΔF_W^{Down} , ΔF_W^{Up} , ΔF_{SW}^{Down} and
 412 ΔF_{SW}^{Up} , Net, LWD, LWU, SWD and SWU, respectively. The central panel shows, for the same
 413 parameters, the corresponding weighted average LWP within 5 W m^{-2} -wide bins of ΔF
 414 ~~radiation anomaly~~ whereas the right panel shows the corresponding count number within 5 W m^{-2} -wide bins fitted by 2 or 3 Gaussian distributions ~~(for no Gaussian distribution when it~~
 415 becomes impossible).

416 Based on our analysis, the relationship between ΔF_{net} , Net ΔSR ($\text{in } \text{W m}^{-2}$) and the LWP
 417 ($\text{in } \text{g m}^{-2}$) has been estimated ~~from the HAMSTRAD and BSRN data~~ as:

$$\Delta F_{net}, \text{Net } \Delta SR(LWP) = -1850.0 (\pm 10.0) + 790.0 \ln(LWP) \quad (914)$$

418 for ΔF_{net} , Net $\Delta SR \in [0 \text{---} 15; 750] \text{ W m}^{-2}$ and $LWP \in [1.25; 3.0] \text{ g m}^{-2}$, where $(\pm 10.0 \text{ W m}^{-2})$
 419 corresponds to the range where the relationship is valid within the ~~two~~two blue dashed lines in
 420 Figure 7-5 centre. Thus, for LWP greater than 1.72 g m^{-2} , our study clearly shows that ~~the there~~

Mis en forme	... [17]
Mis en forme	... [18]
Mis en forme	... [19]
Mis en forme	... [20]
Mis en forme	... [21]
Mis en forme	... [22]
Mis en forme	... [23]
Mis en forme	... [24]
Mis en forme	... [25]
Mis en forme	... [26]
Mis en forme	... [27]
Mis en forme	... [28]
Mis en forme	... [29]
Mis en forme	... [30]
Mis en forme	... [31]
Mis en forme	... [32]
Mis en forme	... [33]
Mis en forme	... [34]
Mis en forme	... [35]
Mis en forme	... [36]
Mis en forme	... [37]
Mis en forme	... [38]
Mis en forme	... [39]
Mis en forme	... [40]
Mis en forme	... [41]
Mis en forme	... [42]
Mis en forme	... [43]
Mis en forme	... [44]
Mis en forme	... [45]
Mis en forme	... [46]
Mis en forme	... [47]
Mis en forme	... [48]
Mis en forme	... [49]
Mis en forme	... [50]
Mis en forme	... [51]
Mis en forme	... [52]
Mis en forme	... [53]
Mis en forme	... [54]
Mis en forme	... [55]
Mis en forme	... [56]
Mis en forme	... [57]
Mis en forme	... [58]
Mis en forme	... [59]
Mis en forme	... [60]
Mis en forme	... [61]
Mis en forme	... [62]
Mis en forme	... [63]
Mis en forme	... [64]
Mis en forme	... [65]
Mis en forme	... [66]

423 is a positive impact of cloud radiative forcing induced by the presence of SLWCs above

424 Concordia is positive on the Net ΔSR that can reach 750 W m⁻² for an LWP of 3.0 g m⁻².

425 The splitting of the net radiation anomaly cloud radiative forcing between each of its four

426 components can be evaluated from their individual relationships with the LWP. These relations

427 are gathered in Table 3, established from the plots presented in Figures 75 to 99. They are of

428 the same form as for net surface radiation anomaly cloud radiative forcing, i.e. a logarithmic

429 dependence on LWP. Table 3 presents the coefficients α and β of the logarithmic function

430 $f(LWP) = \alpha + \beta \ln(LWP)$ for the temperature θT or the radiation components ΔF_{SR} ,

431 together with the valid range of these relations for θT , ΔSR and LWP. For the values presented

432 in Table 3, our study clearly shows that SLWCs have a positive impact on ΔF_{LW}^{Down} and

433 ΔF_{LW}^{Up} , with ΔSR increasing from 0 to 100–90 W m⁻² and from 0 to 40 W m⁻² for LWP ranging

434 from 1.0 to 4.0–3.5 and from 1.6 to 2.5 g m⁻², respectively, a negative impact on ΔF_{SW}^{Down} and

435 ΔF_{SW}^{Up} , decreasing from 0 to -130 and -110 W m⁻², respectively for LWP ranging from 1.5 to

436 4.0 g m⁻², and negligible impact (± 5 W m⁻²) on ΔF_{SW}^{Up} for LWP ranging from 0 to 6.5 g m⁻².

437 Considering the absolute values of ΔF_{SR} vs. LWP relationship (keeping aside ΔF_{SW}^{Up}), it seems

438 that we have systematically one of the most intense Gaussian distributions centred around

439 around at ~ 10 W m⁻², reflecting the non impacting part of SLWCs on SR components, and the

440 other ones centered at ~ 55 W m⁻² and ~ 80 W m⁻².

Mis en forme

Mis en forme : Retrait : Première ligne : 0,75 cm, Taquets de tabulation : Pas à 4,47 cm

Mis en forme

Mis en forme : Surlignage

Mis en forme : Surlignage

Mis en forme

Mis en forme : Retrait : Première ligne : 0,75 cm, Taquets de tabulation : Pas à 4,47 cm

Mis en forme

Mis en forme : Surlignage

Mis en forme

Mis en forme : Retrait : Première ligne : 0,75 cm, Taquets de tabulation : Pas à 4,47 cm

Mis en forme

Mis en forme

Mis en forme : Surlignage

Mis en forme

Mis en forme : Retrait : Première ligne : 0,75 cm, Taquets de tabulation : Pas à 4,47 cm

Mis en forme

Mis en forme : Surlignage

Mis en forme

Mis en forme : Retrait : Première ligne : 0,75 cm, Taquets de tabulation : Pas à 4,47 cm

Mis en forme

Mis en forme : Surlignage

Mis en forme

Mis en forme : Retrait : Première ligne : 0,75 cm, Taquets de tabulation : Pas à 4,47 cm

Mis en forme

Mis en forme : Surlignage

Mis en forme

Mis en forme : Retrait : Première ligne : 0,75 cm, Taquets de tabulation : Pas à 4,47 cm

Mis en forme

Mis en forme : Surlignage

Mis en forme

Mis en forme : Retrait : Première ligne : 0,75 cm, Taquets de tabulation : Pas à 4,47 cm

Mis en forme

Mis en forme : Surlignage

Mis en forme

Mis en forme : Retrait : Première ligne : 0,75 cm, Taquets de tabulation : Pas à 4,47 cm

Mis en forme

Mis en forme : Surlignage

Mis en forme

Mis en forme : Retrait : Première ligne : 0,75 cm, Taquets de tabulation : Pas à 4,47 cm

Mis en forme

Mis en forme : Surlignage

Mis en forme

Mis en forme : Retrait : Première ligne : 0,75 cm, Taquets de tabulation : Pas à 4,47 cm

Mis en forme

Mis en forme : Surlignage

Mis en forme

Mis en forme : Retrait : Première ligne : 0,75 cm, Taquets de tabulation : Pas à 4,47 cm

Mis en forme

Mis en forme : Surlignage

Mis en forme

Mis en forme : Retrait : Première ligne : 0,75 cm, Taquets de tabulation : Pas à 4,47 cm

Mis en forme

Mis en forme : Surlignage

Mis en forme

Mis en forme : Retrait : Première ligne : 0,75 cm, Taquets de tabulation : Pas à 4,47 cm

Mis en forme

Mis en forme : Surlignage

Mis en forme

Mis en forme : Retrait : Première ligne : 0,75 cm, Taquets de tabulation : Pas à 4,47 cm

Mis en forme

Mis en forme : Surlignage

Mis en forme

Mis en forme : Retrait : Première ligne : 0,75 cm, Taquets de tabulation : Pas à 4,47 cm

Mis en forme

Mis en forme : Surlignage

Mis en forme

Mis en forme : Retrait : Première ligne : 0,75 cm, Taquets de tabulation : Pas à 4,47 cm

Mis en forme

Mis en forme : Surlignage

Mis en forme

Mis en forme : Retrait : Première ligne : 0,75 cm, Taquets de tabulation : Pas à 4,47 cm

Mis en forme

Mis en forme : Surlignage

Mis en forme

Mis en forme : Retrait : Première ligne : 0,75 cm, Taquets de tabulation : Pas à 4,47 cm

Mis en forme

Mis en forme : Surlignage

Mis en forme

Mis en forme : Retrait : Première ligne : 0,75 cm, Taquets de tabulation : Pas à 4,47 cm

Mis en forme

Mis en forme : Surlignage

Mis en forme

Mis en forme : Retrait : Première ligne : 0,75 cm, Taquets de tabulation : Pas à 4,47 cm

Mis en forme

Mis en forme : Surlignage

Mis en forme

Mis en forme : Retrait : Première ligne : 0,75 cm, Taquets de tabulation : Pas à 4,47 cm

Mis en forme

Mis en forme : Surlignage

Mis en forme

Mis en forme : Retrait : Première ligne : 0,75 cm, Taquets de tabulation : Pas à 4,47 cm

Mis en forme

Mis en forme : Surlignage

Mis en forme

Mis en forme : Retrait : Première ligne : 0,75 cm, Taquets de tabulation : Pas à 4,47 cm

Mis en forme

Mis en forme : Surlignage

Mis en forme

Mis en forme : Retrait : Première ligne : 0,75 cm, Taquets de tabulation : Pas à 4,47 cm

Mis en forme

Mis en forme : Surlignage

Mis en forme

Mis en forme : Retrait : Première ligne : 0,75 cm, Taquets de tabulation : Pas à 4,47 cm

Mis en forme

Mis en forme : Surlignage

Mis en forme

Mis en forme : Retrait : Première ligne : 0,75 cm, Taquets de tabulation : Pas à 4,47 cm

Mis en forme

Mis en forme : Surlignage

Mis en forme

Mis en forme : Retrait : Première ligne : 0,75 cm, Taquets de tabulation : Pas à 4,47 cm

Mis en forme

Mis en forme : Surlignage

Mis en forme

Mis en forme : Retrait : Première ligne : 0,75 cm, Taquets de tabulation : Pas à 4,47 cm

Mis en forme

Mis en forme : Surlignage

Mis en forme

Mis en forme : Retrait : Première ligne : 0,75 cm, Taquets de tabulation : Pas à 4,47 cm

Mis en forme

Mis en forme : Surlignage

Mis en forme

Mis en forme : Retrait : Première ligne : 0,75 cm, Taquets de tabulation : Pas à 4,47 cm

Mis en forme

Mis en forme : Surlignage

Mis en forme

Mis en forme : Retrait : Première ligne : 0,75 cm, Taquets de tabulation : Pas à 4,47 cm

Mis en forme

Mis en forme : Surlignage

Mis en forme

Mis en forme : Retrait : Première ligne : 0,75 cm, Taquets de tabulation : Pas à 4,47 cm

Mis en forme

Mis en forme : Surlignage

Mis en forme

Mis en forme : Retrait : Première ligne : 0,75 cm, Taquets de tabulation : Pas à 4,47 cm

Mis en forme

Mis en forme : Surlignage

Mis en forme

Mis en forme : Retrait : Première ligne : 0,75 cm, Taquets de tabulation : Pas à 4,47 cm

Mis en forme

Mis en forme : Surlignage

Mis en forme

Mis en forme : Retrait : Première ligne : 0,75 cm, Taquets de tabulation : Pas à 4,47 cm

Mis en forme

Mis en forme : Surlignage

Mis en forme

Mis en forme : Retrait : Première ligne : 0,75 cm, Taquets de tabulation : Pas à 4,47 cm

Mis en forme

Mis en forme : Surlignage

Mis en forme

Mis en forme : Retrait : Première ligne : 0,75 cm, Taquets de tabulation : Pas à 4,47 cm

Mis en forme

Mis en forme : Surlignage

Mis en forme

Mis en forme : Retrait : Première ligne : 0,75 cm, Taquets de tabulation : Pas à 4,47 cm

Mis en forme

Mis en forme : Surlignage

Mis en forme

Mis en forme : Retrait : Première ligne : 0,75 cm, Taquets de tabulation : Pas à 4,47 cm

Mis en forme

Mis en forme : Surlignage

Mis en forme

Mis en forme : Retrait : Première ligne : 0,75 cm, Taquets de tabulation : Pas à 4,47 cm

Mis en forme

Mis en forme : Surlignage

Mis en forme

Mis en forme : Retrait : Première ligne : 0,75 cm, Taquets de tabulation : Pas à 4,47 cm

Mis en forme

Mis en forme : Surlignage

Mis en forme

Mis en forme : Retrait : Première ligne : 0,75 cm, Taquets de tabulation : Pas à 4,47 cm

Mis en forme

Mis en forme : Surlignage

Mis en forme

Mis en forme : Retrait : Première ligne : 0,75 cm, Taquets de tabulation : Pas à 4,47 cm

Mis en forme

Mis en forme : Surlignage

Mis en forme

Mis en forme : Retrait : Première ligne : 0,75 cm, Taquets de tabulation : Pas à 4,47 cm

Mis en forme

Mis en forme : Surlignage

Mis en forme

Mis en forme : Retrait : Première ligne : 0,75 cm, Taquets de tabulation : Pas à 4,47 cm

Mis en forme

Mis en forme : Surlignage

Mis en forme

Mis en forme : Retrait : Première ligne : 0,75 cm, Taquets de tabulation : Pas à 4,47 cm

Mis en forme

Mis en forme : Surlignage

Mis en forme

Mis en forme : Retrait : Première ligne : 0,75 cm, Taquets de tabulation : Pas à 4,47 cm

Mis en forme

Mis en forme : Surlignage

Mis en forme

Mis en forme : Retrait : Première ligne : 0,75 cm, Taquets de tabulation : Pas à 4,47 cm

Mis en forme

Mis en forme : Surlignage

Mis en forme

Mis en forme : Retrait : Première ligne : 0,75 cm, Taquets de tabulation : Pas à 4,47 cm

Mis en forme

Mis en forme : Surlignage

Mis en forme

Mis en forme : Retrait : Première ligne : 0,75 cm, Taquets de tabulation : Pas à 4,47 cm

Mis en forme

Mis en forme : Surlignage

Mis en forme

Mis en forme : Retrait : Première ligne : 0,75 cm, Taquets de tabulation : Pas à 4,47 cm

Mis en forme

Mis en forme : Surlignage

Mis en forme

Mis en forme : Retrait : Première ligne : 0,75 cm, Taquets de tabulation : Pas à 4,47 cm

Mis en forme

Mis en forme : Surlignage

Mis en forme

448 We can also estimate the sensitivity of the longwave component to temperature and
 449 humidity by considering the values of the equivalent atmospheric emissivity ε_a used in the
 450 equations 4-7. On the one side, the values of IWV observed at Dome C are very low even in
 451 summer, typical summertime values are between 0.8 and 1.2 kg m⁻² (Ricaud et al., 2020). This
 452 corresponds to values of ε_a between 0.950 and 0.985, i.e. a relative variation of the order of
 453 3.6%. On the other side, a variation ΔT of the screen-level air (surface) temperature $T_{a_s}(T_s)$ has
 454 a relative impact on the downwelling (upwelling) longwave irradiance of the order of $4 \Delta T/T_s$
 455 ($4 \Delta T/T_s$), which amounts to around 1.6% per degree of ΔT . Given that observations of surface
 456 and screen-level air temperatures reveal variations of several degrees, both in their diurnal cycle
 457 and from a day to another, we can conclude that the impact of temperature on longwave
 458 irradiance variations is larger than that of IWV.

459 Furthermore, our study also shows that SLWCs have a clear negative impact on SWD and
 460 SWU, with ASR decreasing from 0 to 140 W m⁻² and from 0 to 75 W m⁻² with LWP ranging
 461 from 1.2 to 3.8 and from 1.2 to 3.2 g m⁻², respectively.

462 463 5. Discussion

464 5.1 Relation with critical temperature

465 Note that the relationships show an exponential dependence of LWP on both temperature
 466 and SR anomaly. Similarly similar to the dependence of the molar volume and density of water
 467 on critical temperature. As a matter of fact, the density ρ (g cm⁻³) and molar volume v (cm³
 468 mol⁻¹) of liquid water are exponentially varying with temperature (Sippola and Taskinen, 2018):

$$469 \rho = \rho_0 \exp\{-T_c(A + B\varepsilon_0 + 2C\varepsilon_0^{1/2}e^{1/2})\} \quad (1315)$$

$$470 v = \frac{M_{H_2O}}{\rho} = \frac{M_{H_2O}}{\rho_0} \exp\{T_c(A + B\varepsilon_0 + 2C\varepsilon_0^{1/2}e^{1/2})\} \quad (1416)$$

Mis en forme : Surlignage

471 where ρ_0 (g cm⁻³), A (K⁻¹), B (K⁻¹), and C (K⁻¹) are parameters; T_c is the critical temperature
472 whose value varies from 227 to 228 K, and M_{H_2O} (g mol⁻¹) is the molecular weight of water.

473 $\varepsilon_0\varepsilon$ (unitless) is defined as:

$$\varepsilon_0\varepsilon = \frac{T}{T_c} - 1 \quad (1517)$$

475 where T is temperature in K.

Mis en forme : Surlignage
Mis en forme : Surlignage
Mis en forme : Surlignage
Mis en forme : Surlignage

476

477 *5.2. Reference Surface Radiation and sastrugi effect*

478 In order to evaluate the surface radiation in clear-sky conditions at Concordia, we have
479 used, in complement to BSRN observations, and at the closest location to Concordia station,
480 two different data sets of surface radiations from i) the European Center for Medium-Range
481 Weather Forecasts Reanalysis version 5 (ERA5). ERA5 is a climate reanalysis dataset, covering
482 the period 1979 to present. ERA5 is being developed through the Copernicus Climate Change
483 Service (C3S). Extracted data (<https://cds.climate.copernicus.eu/cdsapp#!/dataset/reanalysis-era5-single-levels>) used here are hourly at a regular horizontal grid of 0.25°x0.25° in clear-sky
484 conditions: surface solar and thermal infrared, downward and net radiations. As explained on
485 the ERA5 website, clear-sky radiations are computed for the same atmospheric conditions of
486 temperature, humidity, ozone, trace gases and aerosol as the corresponding total sky quantities
487 (clouds included), but assuming that the clouds are not there; ii) the Clouds and the Earth's
488 Radiant Energy System (CERES), containing SYN1deg (Hourly CERES and geostationary
489 (GEO) TOA fluxes, MODIS/VIIRS and GEO cloud properties, MODIS/VIIRS aerosols, and
490 Fu Liou radiative transfer surface and in atmospheric (profile) fluxes consistent with the
491 CERES observed TOA fluxes, as explained on <https://ceres.larc.nasa.gov/data/>). Surface fluxes
492 in SYN1deg are computed with cloud properties derived from MODIS and geostationary
493 satellites (GEO), where each geostationary satellite instrument is calibrated against MODIS

Mis en forme : Espacement automatique entre les caractères
asiatiques et latins, Espacement automatique entre les
caractères asiatiques et les chiffres, Taquets de tabulation :
4,47 cm, Gauche

495 (Doelling et al. 2013; 2016) at $1^\circ \times 1^\circ$ horizontal resolution (<https://ceres.larc.nasa.gov/data/>).

496 Aerosol and atmospheric data were included as inputs to calculate the radiation flux.

497 We have compared the CERES and ERA5 data with the BSRN hourly averaged data on
498 the 5 reference days (clear sky conditions) for the Net, LWD, LWU, SWD and SWU SRs.
499 Figure 10 shows these variables for the 26 December 2021. The LWD and LWU values show
500 an overall consistency between ERA5 and CERES (of the order of 10 W m^{-2}), while a
501 systematic negative bias of $-20\text{--}40 \text{ W m}^{-2}$ is observed with respect to BSRN data. However,
502 the net longwave radiation, i.e. the difference LWD – LWU for each data set, is reduced to
503 around 5 W m^{-2} . The SWD and SWU signals from ERA5, CERES and BSRN show a similar
504 diurnal variation with differences less than 50 W m^{-2} . When considering the Net SR, some
505 obvious differences up to 50 W m^{-2} can be seen between BSRN, ERA5 and CERES. Since the
506 net longwave radiation is within 10 W m^{-2} for the three data sets, the source of this difference
507 therefore should come from either SWD or SWU radiation. We have calculated, for BSRN,
508 ERA5 and CERES data, the albedo defined as:

509
$$\text{albedo} = \frac{\text{SWU}}{\text{SWD}} \quad (10)$$

510 Figure 11 shows the diurnal evolution of the albedo on 26 December 2021 (clear sky day).
511 The CERES and ERA5 albedos do not show any significant diurnal variation with quite
512 constant values of 0.74 and 0.83, respectively, whilst the observed BSRN albedo shows a clear
513 diurnal signal with a maximum of 0.85 from 10:00 to 14:00 UTC (from 18:00 to 22:00 LT) and
514 a minimum of 0.70 from 19:00 to 23:00 UTC (from 03:00 to 07:00 LT). The large diurnal signal
515 present in the observed albedo is likely the signature of the sastrugi effect that is obviously
516 absent in the ERA5 and CERES data sets. The BSRN SWU sensor has a circular footprint. For
517 a sensor installed at a height h above the ground, 90% of the signal comes from an area at the
518 surface closer than $3.1 \cdot h$ (Kassianov et al., 2014). Since at Dome C the instrument is installed

519 at a height of 2-3 m, the albedo is thus determined by the surface elements in the immediate
520 vicinity (a few meters) of the sensor.

521 Sastrugi (Figure 12) are features formed by erosion of snow by wind. They are found in
522 polar regions, and in snowy, wind swept areas of temperate regions, such as frozen lakes or
523 mountain ridges. Sastrugi are distinguished by upwind facing points, resembling anvils, which
524 move downwind as the surface erodes.

525 We have fitted the BSRN albedo averaged over the 5 reference days with the sum of 2 sine
functions, imposing periods of 24 and 12 hours. Figure 13 shows the BSRN albedo averaged
526 over the five clear sky days, the fitted trigonometric function and the residuals between the
527 averaged albedo and the fitted function. We can state that the sastrugi effect on the observed
528 clear sky albedo at Concordia is successfully fitted by 2 sine functions of 24h and 12h periods
529 to within 0.003 mean absolute error, with a coefficient of determination R^2 equal to 0.993 and
530 a root mean square error of 0.0004.

532 If we suppose that the sastrugi effect impacts mostly SWU rather than SWD, and the albedo
533 calculated from BSRN observations is the “truth”, we can calculate a modified SWU*
534 (including the sastrugi effect) for the ERA5 and CERES as:

$$535 \quad SWU(ERA5)^* = SWD(ERA5) \times \text{albedo}(BSRN) \quad (11)$$

$$536 \quad SWU(CERES)^* = SWD(CERES) \times \text{albedo}(BSRN) \quad (12)$$

537 Then we calculate the modified Net SR* (including the sastrugi effect) considering SWU* for
538 ERA5 and CERES. As an example, we present Figure 14, similar to Figure 10, in which we
539 added the albedo and the SWU* and Net SRs* (including the sastrugi effect) for CERES and
540 ERA5 (solid lines). We observe that the Net SR* for ERA5 and CERES now coincides with
541 the BSRN Net SR to within 5 W m^{-2} , compared to differences up to 50 W m^{-2} found when the
542 sastrugi effect was not taken into account.

Mis en forme : Retrait : Première ligne : 0 cm

543 Moreover, we have considered all the BSRN observations in December 2018, 2019, 2020
544 and 2021 to calculate the albedo (Figure 15), and we have superimposed the fitted trigonometric
545 function as described in Figure 13. The presence of clouds is well highlighted by observations
546 that depart from the fitted function whilst, during periods of clear sky conditions, BSRN
547 albedos coincide well with the fitted function.

548 ~~The study we have performed was extremely fruitful to evaluate the impact of the SLW~~
549 ~~clouds on the SR. The methodology requires reference clear sky SR values that can be~~
550 evaluated from: 1) models, 2) analyses and 3) observations. Our study has mainly shown that,
551 at the Concordia station, sastrugi were present and strongly impacted the net SR via the surface
552 albedo. This very local phenomenon cannot be taken into account by either the global scale
553 analyses (ERA5 and CERES), or standard radiative transfer models (e.g. RRTMG). As a
554 consequence, the methodology we have developed based on field observations is likely the most
555 powerful tool to estimate the Net SR in Concordia. It has some drawbacks, as for instance some
556 biases for LWD and LWU between analyses and observations, but the LWD and LWU
557 difference used to calculate the Net SR dramatically lessens the bias.

558 5.3.2 Modelling SLWC

Mis en forme : Surlignage

559 Previous studies have already underlined the difficulty to model the SLWC together with
560 its impact on surface radiations. Modelling SLWCs over Antarctica is challenging because 1)
561 operational observations are scarce since the majority of meteorological radiosondes are
562 released from ground stations located at the coast and very few of them are maintained all year
563 long, and satellite observations are limited to 60°S in geostationary orbit whilst, in a polar orbit,
564 the number of available orbits does not exceed 15 per day, and 2) the model should provide a
565 partition function favouring liquid water at the expense of ice for temperatures between -36°C
566 and 0°C in order to calculate realistic SLW contents. Differences of 20 to 50 W m⁻² in the Net
567 SR-surface irradiance were found in the Arpege model (Pailleux et al., 2015) between clouds

Mis en forme : Surlignage

568 made of ice or liquid water during the summer 2018-2019 (Ricaud et al., 2020), differences that
569 are very consistent with the results obtained in the present study. Although SLWCs are less
570 present over the Antarctic Plateau than over the coastal region, their radiative impact is not
571 negligible and should be taken into account with great care in order to estimate the radiative
572 budget of the Antarctic continent in one hand, and, on the other hand, over the entire Earth.

573 **5.4. Errors**

574 Measurements of temperature, LWP, depolarization signal and ~~SR~~surface irradiances F
575 are altered by random and systematic errors that may affect the relationships we have obtained
576 between LWP and either temperature or ~~SR~~anomalies cloud radiative forcing ΔF. The
577 temperature measured by HAMSTRAD below 1 km has been evaluated against radiosonde
578 coincident observations from 2009 to 2014 (Ricaud et al., 2015) and the resulting bias is 0-2°C
579 below 100 m and between -2 and 0°C between 100 and 1000 m. SLWCs are usually located
580 around 400-600 m above the ground where the cold bias can be estimated to be about -1.0°C.
581 The one-sigma ($1-\sigma$) RMS temperature error over a 7-min integration time is 0.25°C in the PBL
582 and 0.5°C in the free troposphere (Ricaud et al., 2015). As a consequence, given the number of
583 points used in the statistical analysis (>1000), the random error on the weighted-average
584 temperature is negligible (<0.02°C). The LWP random and systematic errors are difficult to
585 evaluate since there is no coincident external data to compare with. Nevertheless, the $1-\sigma$ RMS
586 error over a 7-min integration time can be estimated to be 0.25 g m⁻² giving a random error on
587 the weighted average LWP less than 0.08 g m⁻². Based on clear-sky observations, the positive
588 bias can be estimated to be of the order of less than 0.4 g m⁻². Theoretically, SLW should not
589 exist at temperatures less than -39°C although it has been observed in recent laboratory
590 measurements down to -42.55°C (Goy et al., 2018). Using equation (813) with an LWP bias of
591 0.4 g m⁻² gives a temperature of -39.8°C (~0.8°C lower than the theoretical limit of -39°C), so
592 the biases estimated for temperature and LWP are very consistent with theory.

Mis en forme : Surlignage

The estimation of systematic and random errors on LIDAR backscattering and depolarization signals and their impact on the attribution/selection of SLWC is not trivial. But the most important point is to evaluate whether the observed cloud is constituted of purely liquid or mixed-phase water. Even considering the backscatter intensity only, we could not exclude that ice particles could have been present in the SLWC events investigated in 2018 (Ricaud et al., 2020). Therefore, in the present analysis, although we made a great attention to diagnose ice in the LIDAR cloud observations, we cannot totally exclude ice particles thus mixed-phase parcels were actually present when we labelled the observed cloud as SLWCs.

The 4 instruments providing- $F_{\text{LW}}^{\text{Down}}$, $F_{\text{LW}}^{\text{Up}}$, $F_{\text{SW}}^{\text{Down}}$ and $F_{\text{SW}}^{\text{Up}}$ LWD, LWU, SWD and SWU
 SR follow the rules of acquisition, quality check and quality control of the BSRN (Driemel et
 al., 2018). These data are often considered as a reference against which products based on
 satellite observations and radiative transfer models (such as e.g. CERES) are validated (Kratz
 et al., 2020). In polar regions (Lanconelli et al., 2011), $F_{\text{SW}}^{\text{Down}}$ and $F_{\text{SW}}^{\text{Up}}$ SWU and SWD SRs
 are expected to be affected by random errors up to $\pm 20 \text{ W m}^{-2}$ while $F_{\text{LW}}^{\text{Down}}$ LWD SRs are
 expected to be affected by random errors not greater than $\pm 10 \text{ W m}^{-2}$ (Ohmura et al., 1998). As
 a consequence, given the large number of observations used per 5 W m^{-2} -wide bins (1000-
 3000), the random error on the weighted-average SRFs is negligible ($0.3\text{-}0.7 \text{ W m}^{-2}$) whatever
 the radiations considered, LW and SW.

Finally, ~~apart from the instrument related SR_{ref} error~~, another source of error comes from 1) the geometry of observation and 2) the discontinuous SLWC layer. Firstly, LIDAR is almost zenith pointing, HAMSTRAD makes a scan in the East direction (from 10° elevation to zenith), whilst the BSRN radiometers detect the radiation in a 2π -steradians field of view (3D configuration). That is to say, in our analysis, the whole sky contributes to the radiation whilst only the cloud at zenith (1D configuration) and on the East direction (2D configuration) is

617 observed by the LIDAR and HAMSTRAD, respectively. Secondly, SLWCs cannot be
618 considered as uniform in the whole (see e.g. broken cloud fields in Figure 2).

619 **5.3.4 Other clouds**

Mis en forme : Surlignage

620 Although the method we have developed to select the SLWCs has been validated using the
621 amount of LWP and, in another study, using space-borne observations (Ricaud et al., 2020), we
622 cannot rule out that, associated with the SLW droplets, are also ice particles, that is clouds are
623 constituted of a mixture of liquid and solid water. [Statistics of ice and mixed-phase clouds over](#)
624 [the Antarctic Plateau have been performed by Cossich et al. \(2021\) revealing mean annual](#)
625 [occurrences of 72.3 %, 24.9 %, and 2.7 % for clear sky, ice clouds, and mixed-phase clouds,](#)
626 [respectively.](#) Generally, [such mixed-phase clouds are a superposition of a lower layer being](#)
627 made of liquid water and an upper layer being made of solid water (see Fig. 12.3 from Lamb
628 and Verlinde, 2011). These mixed-layer clouds do not significantly modify the relationship
629 between temperature and LWP because 1) SLW observations from HAMSTRAD are only
630 sensitive to water in liquid phase and 2) temperature from HAMSTRAD is selected at times
631 and vertical heights where the LIDAR depolarization signal is very low (<5%). Although we
632 have verified that pure ice clouds were not selected by our method, we cannot differentiate
633 mixed-phase clouds from purely SLWCs. [As a consequence, the presence of mixed phase](#)
634 [clouds in addition to SLWCs may explain the negative part of the Net, LWD and LWU ASR](#)
635 [\(\[-20;0\] W m⁻²\) and the positive part of the SWD and SWU ASR \(\[0;10\] W m⁻²\) for low](#)
636 [values of LWP \(\[0.8;1.6\] g m⁻²\).](#)

637 Furthermore, we already have noticed that SLWCs developed at the top of the PBL (Ricaud
638 et al., 2020) in the “entrainment zone” and maintained in the “capping inversion zone”,
639 following the terminology of Stull (1988), at a height ranging from 100 to 1000 m above ground
640 level. Nevertheless, [during the local “night” at 00:00-06:00 LT, when the sun is at low elevation](#)
641 [above the horizon \(24-h polar day\)](#), the PBL may collapse down to a very low height ranging

642 20-50 m. In this configuration, it is hard to differentiate from LIDAR observations between a
643 SLWC and a fog episode, although the LIDAR can measure depolarization (but not backscatter)
644 down to approximately 10-30 m above the ground (Figure S3 in Chen et al., 2017), so that we
645 can distinguish liquid/frozen clouds very close to the ground.

646 Finally, we cannot rule out that, above the SLWCs that are actually observed by both
647 LIDAR and HAMSTRAD, other clouds might be present, as e.g. cirrus clouds constituted of
648 ice crystals. These mid-to-upper tropospheric clouds cannot be detected by HAMSTRAD (no
649 sensitivity to ice crystals). In the presence of SLWCs either low in altitude or optically thick,
650 the LIDAR backscatter signal is decreased in order to avoid saturation and the signal from upper
651 layers is thus almost cancelled. These mid-to-high-altitude clouds are **observed-sensed** by the Mis en forme : Surlignage
652 BSRN instruments and **SR-surface irradiance** can be affected in this configuration. Based on Mis en forme : Surlignage
653 the presence of cirrus clouds before or after the SLWCs (and sometimes during the SLWCs if
654 optically thin), we can estimate that the number of days when SLWCs and cirrus clouds are
655 simultaneously present to cover less than 10% of our period of interest.

656 **5.5. Sastrugi effect on the surface albedo**

657 **Sastrugi** (Figure 10) are features formed by erosion of snow by wind. They are found in
658 polar regions, and in snowy, wind-swept areas of temperate regions, such as frozen lakes or
659 mountain ridges. Sastrugi are distinguished by upwind-facing points, resembling anvils, which
660 move downwind as the surface erodes.

661 **Figure 11** shows the BSRN surface albedo averaged over the five cloud-free days (2 and Mis en forme : Surlignage
662 19 December 2018; 3, 17 and 26 December 2021) showing a clear diurnal signal with a Mis en forme : Surlignage
663 maximum of 0.85 from 10:00 to 14:00 UTC (from 18:00 to 22:00 LT) and a minimum of 0.70
664 from 19:00 to 23:00 UTC (from 03:00 to 07:00 LT). The large diurnal signal present in the
665 observed surface albedo is likely the signature of the sastrugi effect. The BSRN SWU sensor
666 has a circular footprint. For a sensor installed at a height h above the ground, 90% of the signal

667 comes from an area at the surface closer than 3.1 h (Kassianov et al., 2014). Since at Dome-C
668 the instrument is installed at a height of 2-3 m, the albedo is thus determined by the surface
669 elements in the immediate vicinity (a few meters) of the sensor.

670 We have fitted the averaged cloud-free BSRN surface albedo with the sum of two sine
671 functions, imposing periods of 24 and 12 hours (Figure 11) together with the residuals between
672 the averaged surface albedo and the fitted function. We can state that the sastrugi effect on the
673 observed cloud-free surface albedo at Concordia is successfully fitted by two sine functions of
674 24h and 12h periods to within 0.003 mean absolute error, with a coefficient of determination
675 R^2 equal to 0.993 and a root mean square error of 0.0004.

Mis en forme : Surlignage

Mis en forme : Surlignage

Mis en forme : Surlignage

676 Moreover, we have considered all the BSRN observations in Decembers 2018, 2019, 2020
677 and 2021 to calculate the albedo (Figure 12), and we have superimposed the fitted trigonometric
678 function as described in Figure 11. The presence of clouds is well highlighted by observations
679 that depart from the fitted function whilst, during periods of clear-sky conditions, BSRN
680 albedos coincide well with the fitted function. To conclude, the surface albedo at Concordia
681 should be treated considering sastrugi effect.

Mis en forme : Ne pas ajuster l'espace entre le texte latin et
asiatique, Ne pas ajuster l'espace entre le texte et les
nombres asiatiques, Taquets de tabulation : Pas à 4,47 cm

Mis en forme : Surlignage

Mis en forme : Anglais (États-Unis), Surlignage

682 5.66. Maximum Potential radiative impact SLWC Radiative Forcing of SLWCs over Antarctica

Mis en forme : Surlignage

683 Based on 2007-2010 reanalyses, observations and climate models (Lenaerts et al., 2017),
684 LWP over Antarctica is on average less than 10 g m^{-2} , with slightly larger values in summer
685 than in winter by $2\text{-}5 \text{ g m}^{-2}$. Over Western Antarctica, LWPs are larger ($20\text{-}40 \text{ g m}^{-2}$) than over
686 Eastern Antarctica ($0\text{-}10 \text{ g m}^{-2}$). As a consequence, LWPs observed at Concordia are consistent
687 with values observed over the Eastern Plateau, with a factor 2-4 smaller than those observed
688 over the Western continent. Based on our results and on the observed cloud fraction (η_{CF}) of
689 SLWCs over Antarctica for different seasons (Listowski et al., 2019), we have can estimated
690 the potential maximum radiative impact of SLWCs SLWC radiative forcing at the scale of the

691 Antarctic continent ($\Delta F_{Net-Ant}^{max} \Delta SR_{Net-Ant global}^{max}$) from the maximum of $\Delta F_{Net-Ant}$, $\Delta SR_{Net-Ant}$
 692 ($\Delta F_{Net-Ant}^{max} \Delta SR_{Net-Ant}^{max} = 750 \text{ W m}^{-2}$) computed in our study:
 693
$$\Delta F_{Net-Ant}^{max} \Delta SR_{Net-Ant global}^{max} = \eta_{CF} \times \Delta F_{Net}^{max} \times Net \Delta SR^{max}$$
 (1318)

Mis en forme : Surlignage

Mis en forme

[... [77]]

Mis en forme

[... [78]]

Mis en forme

[... [79]]

Mis en forme

[... [80]]

694 In summer, η_{CF} is varying from 5% in Eastern Antarctica to 40% in Western Antarctica whilst,
 695 in winter, it is varying from 0% in Eastern Antarctica to 20% in Western Antarctica (Listowski
 696 et al., 2019). In December, if we consider η_{CF} for SLW-containing cloud (that is to say both
 697 mixed-phase cloud and unglaciated SLW cloud consistent with our study), we find for a lower-
 698 level altitude cut-off of 0, 500 and 1000 m (Figure B1 in Listowski et al., 2019), a potential
 699 maximum SLWC radiative impact forcing $\Delta F_{Net-Ant}^{max} \Delta SR_{Net-Ant global}^{max}$ over Antarctica of about
 700 912, 710 and 57 W m⁻², respectively. We now separate the Eastern elevated Antarctic Plateau
 701 from the Western Antarctica (Figure 5 in Listowski et al., 2019) for the 4 seasons. Over Eastern
 702 Antarctica, we find that $\Delta F_{Net-Ant}^{max} \Delta SR_{Net-Ant global}^{max} = 0.70.5-57.0 \text{ W m}^{-2}$ in December-January-
 703 February (DJF) and 0-32.5 W m⁻² for the remaining seasons. Over Western Antarctica, the
 704 potential maximum radiative impact is much more intense because of higher temperatures and
 705 lower elevations compared to the Eastern Antarctic Plateau: $\Delta F_{Net-Ant}^{max} \Delta SR_{Net-Ant global}^{max} = 172.5$
 706 430.0 W m⁻² in DJF (30-40 W m⁻² over the Antarctica Peninsula); 107.5-280.0 W m⁻² in March-
 707 April-May; 32.5-140.0 W m⁻² in June-July-August; and 75.0-172.5 W m⁻² in September-
 708 October-November. To summarize, the maximum SLWC radiative forcing over Western
 709 Antarctica (0-40 W m⁻²) is estimated to 3 to 5 times larger compared to the one over the Eastern
 710 Antarctic Plateau (0-7 W m⁻²), maximizing during the summer season.

Mis en forme : Surlignage

Mis en forme

[... [81]]

Mis en forme

[... [82]]

Mis en forme

[... [83]]

712 6. Conclusions

713 Combining the observations of temperature, water vapour and liquid water path from a
 714 ground-based microwave radiometer, backscattering and depolarization from a ground-based
 715 LIDAR, screen-level air temperature and surface radiations at long and short wavelengths, our

Mis en forme : Surlignage

716 analysis has been able to evaluate the presence of supercooled liquid water clouds over the
717 Dome C station in summer. Focusing on the month of December in 2018-2021, we established
718 that in SLWCs temperature logarithmically increases from -36.0°C to -16.0°C when LWP
719 increases from 1.0 to 14.0 g m⁻². We have also evaluated that SLWCs positively affect the net

720 ~~SRadiative forcing~~, which logarithmically increases from 0.0 to ~~5070.0 W m⁻²~~ when LWP
721 increases from ~~1.72~~ to ~~3.05~~ g m⁻². Our study clearly shows that SLWCs have a positive impact
722 on ΔF_{LW}^{Down} , increasing from 0 to 90 W m⁻² for LWP ranging from 1.0 to 3.5 g m⁻², a negligible
723 impact (± 5 W m⁻²) on ΔF_{LW}^{Up} for LWP ranging from 0 to 6.5 g m⁻², and a negative (but quite
724 offsetting) impact on each of the two terms ΔF_{LW}^{Down} and ΔF_{LW}^{Up} , which decrease from 0 to -130
725 and -110 W m⁻², respectively for LWP ranging from 1.5 to 4.0 g m⁻². This means that the impact
726 of SLWC on the net radiative forcing is mainly driven by the downward surface irradiance since
727 the attenuation of solar incoming irradiance is almost compensated for by the upward shortwave
728 irradiance because of high values of surface albedo. Our study clearly shows that: 1) SLWCs
729 have a positive impact on LWD and LWU, with ΔSR increasing from 0 to 100 W m⁻² and from
730 0 to 40 W m⁻² for LWP ranging from 1.0 to 4.0 and from 1.6 to 2.5 g m⁻², respectively, and 2)
731 SLWCs have a clear negative impact on SWD and SWU, with ΔSR decreasing from 0 to -140
732 W m⁻² and from 0 to -75 W m⁻² with LWP ranging from 1.2 to 3.8 and from 1.2 to 3.2 g m⁻²,
733 respectively.

734 Our study has mainly shown that, at the Concordia station, sastrugi were present and
735 strongly impacted the net SR via the surface albedo. This very local phenomenon cannot be
736 taken into account by either the global scale analyses (ERA5 and CERES), or standard radiative
737 transfer models. As a consequence, the methodology we have developed based on field
738 observations is likely the most powerful tool to estimate the Net SR in Concordia. It has some
739 drawbacks, as for instance some biases for LWD and LWU between analyses and observations,

Mis en forme : Surlignage

Mis en forme : Anglais (États-Unis)

740 but the LWD—LWU difference that is used to calculate the Net SR dramatically lessens the
741 bias.

742 Finally, extrapolating our results of the SLWC radiative impact forcing of the SLWCs from
743 the Dome C station to the Antarctic continent shows that SLWCs have a great the potential
744 maximum SLWC radiative impact forcing is not greater than all over Antarctica whatever the
745 season considered, up to 75.0 W m^{-2} over the Eastern Antarctic Plateau and but 2 to 3 times
746 larger (up to 430 W m^{-2}) over the Western Antarctica, maximizing over in summer season and
747 over the Antarctic Peninsula in summer season. This stresses the importance of accurately
748 modelling SLWCs when calculating the Earth energy budget to adequately forecast the Earth
749 climate evolution, especially since the climate is rapidly changing in Antarctica, as illustrated
750 by the surface temperature record of -12°C recently observed in March 2022 at the Concordia
751 station and largely publicized worldwide (see e.g. <https://www.9news.com.au/world/antarctica-heatwave-extreme-warm-weather-recorded-concordia-research-station/3364dd91-2051-4df5-8efe-5f2819058604>).
755

756 Data availability

757 HAMSTRAD data are available at <http://www.cnrm.meteo.fr/spip.php?article961&lang=en>
758 (last access: 3 May 2022). The tropospheric depolarization LIDAR data are reachable at
759 <http://lidarmax.altervista.org/lidar/home.php> (last access: 3 May 2022). Radiosondes are
760 available at <http://www.climantartide.it> (last access: 3 May 2022). Screen-level air temperature
761 from AWS can be obtained from the ftp server
762 (<https://amrc.ssec.wisc.edu/data/archiveaws.html>) (last access: 17 October 2023). BSRN data
763 can be obtained from the ftp server (<https://bsrn.awi.de/data/data-retrieval-via-ftp/>) (last access:
764 3 May 2022).

765

766 **Author contribution**

767 PR, MDG, and AL provided the observational data. PR developed the methodology. All the
768 co-authors participated in the data analysis and in the data interpretation. PR prepared the
769 manuscript with contributions from all co-authors.

770

771 **Competing interests**

772 The authors declare that they have no conflict of interest.

773

774 **Acknowledgments**

775 The present research project Water Budget over Dome C (H2O-DC) has been approved by
776 the Year of Polar Prediction (YOPP) international committee. The HAMSTRAD programme
777 (910) was supported by the French Polar Institute, Institut polaire français Paul-Emile Victor
778 (IPEV), the Institut National des Sciences de l'Univers (INSU)/Centre National de la Recherche
779 Scientifique (CNRS), Météo-France and the Centre National d'Etudes Spatiales (CNES). The
780 permanently manned Concordia station is jointly operated by IPEV and the Italian Programma
781 Nazionale Ricerche in Antartide (PNRA). The tropospheric LIDAR operates at Dome C from
782 2008 within the framework of several Italian national (PNRA) projects. We would like to thank
783 all the winterover personnel who worked at Dome C on the different projects: HAMSTRAD,
784 aerosol LIDAR and BSRN. We would like to thank the ~~two-three~~ anonymous reviewers for
785 their beneficial comments.

786

787 **References**

788 Bergeron, T., 1928: Über die dreidimensional verknüpfende Wetteranalyse. – Geophys. Norv.

Mis en forme : Surlignage

789 [Branch, M. A., T. F. Coleman, and Y. Li: A Subspace, Interior, and Conjugate Gradient Method](#)
790 for Large-Scale Bound-Constrained Minimization Problems, SIAM Journal on Scientific
791 Computing, 21, 1, 1-23, 1999.

Mis en forme : Surlignage

Mis en forme : Anglais (États-Unis)

792 Bromwich, D. H., Nicolas, J. P., Hines, K. M., Kay, J. E., Key, E. L., Lazzara, Lubin, D.,
793 McFarquhar, G. M., Gorodetskaya, I. V., Grosvenor, D. P., Lachlan-Cope, T., and van
794 Leipzig, N. P. M.: Tropospheric clouds in Antarctica, Rev. Geophys., 50, RG1004,
795 <https://doi.org/10.1029/2011RG000363>, 2012.

796 Bromwich, D. H., Otieno, F. O., Hines, K. M., Manning, K. W., and Shilo, E.: Comprehensive
797 evaluation of polar weather research and forecasting model performance in the Antarctic, J.
798 Geophys. Res.-Atmos., 118, 274–292, 2013.

799 Chen, X., Virkkula, A., Kerminen, V.-M., Manninen, H. E., Busetto, M., Lanconelli, C., Lupi,
800 A., Vitale, V., Del Guasta, M., Grigioni, P., Väänänen, R., Duplissy, E.-M., Petäjä, T., and
801 Kulmala, M.: Features in air ions measured by an air ion spectrometer (AIS) at Dome C,
802 Atmos. Chem. Phys., 17, 13783–13800, <https://doi.org/10.5194/acp-17-13783-2017>, 2017.

803 [Clough, S. A., M. W. Shephard, E. J. Mlawer, J.S. Delamere, M. J. Iacono, K. Cady-Pereira, S.](#)
804 [Beckerman, and P. D. Brown. Atmospheric radiative transfer modeling: A summary of the](#)
805 [aer codes. J. Quant. Spectrosc. Radiat. Transfer, 91:233–244, 2005.](#) [Cossich, W., Macestri,](#)
806 [T., Magurno, D., Martinazzo, M., Di Natale, G., Palchetti, L., Bianchini, G., and Del Guasta,](#)
807 [M.: Ice and mixed-phase cloud statistics on the Antarctic Plateau, Atmos. Chem. Phys., 21,](#)
808 [13811–13833, https://doi.org/10.5194/acp-21-13811-2021, 2021.](#)

Mis en forme : Surlignage

809 [Deepling, D. R., N. G. Loeb, D. F. Keyes, M. L. Nordeen, D. Morstad, C. Nguyen, B. A.](#)
810 [Wielicki, D. F. Young, M. Sun, 2013: Geostationary Enhanced Temporal Interpolation for](#)
811 [CERES Flux Products, Journal of Atmospheric and Oceanic Technology, 30\(6\), 1072–1090.](#)
812 [doi:10.1175/JTECH-D-12-00136.1.](#)

- 813 Deelling, D. R., M. Sun, L. T. Nguyen, M. L. Nørdeen, C. O. Haney, D. F. Keyes, P. E.
814 Mlynczak, 2016: Advances in Geostationary Derived Longwave Fluxes for the CERES
815 Synoptic (SYN1deg) Product, *Journal of Atmospheric and Oceanic Technology*, 33(3),
816 503–521. doi: 10.1175/JTECH-D-15-0147.1.
- 817 Driemel, A., Augustine, J., Behrens, K., Colle, S., Cox, C., Cuevas-Agulló, E., Denn, F. M.,
818 Duprat, T., Fukuda, M., Grobe, H., Haeffelin, M., Hodges, G., Hyett, N., Ijima, O., Kallis,
819 A., Knap, W., Kustov, V., Long, C. N., Longenecker, D., Lupi, A., Maturilli, M., Mimouni,
820 M., Ntsangwane, L., Ogihara, H., Olano, X., Olefs, M., Omori, M., Passamani, L., Pereira,
821 E. B., Schmithüsen, H., Schumacher, S., Sieger, R., Tamlyn, J., Vogt, R., Vuilleumier, L.,
822 Xia, X., Ohmura, A., and König-Langlo, G.: Baseline Surface Radiation Network (BSRN):
823 structure and data description (1992–2017), *Earth Syst. Sci. Data*, 10, 1491–1501,
824 https://doi.org/10.5194/essd-10-1491-2018, 2018.
- 825 Dupont, J.C., Haeffelin, M., Drobinski, P. and Besnard, T.: Parametric model to estimate clear-
826 sky longwave irradiance at the surface on the basis of vertical distribution of humidity and
827 temperature. *Journal of Geophysical Research: Atmospheres*, 113(D7),
828 https://doi.org/10.1029/2007JD009046, 2008.
- 829 Dutton, E.G., Farhadi, A., Stone, R.S., Long, C.N. and Nelson, D.W.: Long-term variations in
830 the occurrence and effective solar transmission of clouds as determined from surface-based
831 total irradiance observations. *Journal of Geophysical Research: Atmospheres*, 109(D3),
832 https://doi.org/10.1029/2003JD003568, 2004.
- 833 Findeisen, W., 1938: Kolloid-meteorologische Vorgänge bei Niederschlagsbildung. *Meteorol.*
834 Z. 55, 121–133. (translated and edited by Volken, E., A.M. Giesche, S. Brönnimann. –
835 Meteorol. Z. 24 (2015), DOI:10.1127/metz/2015/0675).

Mis en forme : Justifié, Retrait : Gauche : 0 cm, Suspendu : 0,63 cm, Interligne : Double, Taquets de tabulation : 4,47 cm, Gauche

Mis en forme : Surlignage

Mis en forme : Anglais (États-Unis)

Mis en forme : Surlignage

Mis en forme : Anglais (États-Unis)

- 836 [Gardner, A.S. and Sharp, M.J.: A review of snow and ice albedo and the development of a new](#)
- 837 [physically based broadband albedo parameterization. Journal of Geophysical Research:](#)
- 838 [Earth Surface, 115\(F1\), 2010.](#)
- 839 Goy, C., Potenza, M. A., Dedera, S., Tomut, M., Guillerm, E., Kalinin, A., Voss, K.-O.,
- 840 Schottelius, A., Petridis, N., Prosvetov, A., Tejeda, G., Fernández, J. M., Trautmann, C.,
- 841 Caupin, F., Glasmacher, U., and Grisenti, R. E.: Shrinking of rapidly evaporating water
- 842 microdroplets reveals their extreme supercooling, Phys. Rev. Lett., 120, 015501,
- 843 <https://doi.org/10.1103/PhysRevLett.120.015501>, 2018.
- 844 Grazioli, J., Genthon, C., Boudevillain, B., Duran-Alarcon, C., Del Guasta, M., Madeleine, J.-
- 845 B., and Berne, A.: Measurements of precipitation in Dumont d'Urville, Adélie Land, East
- 846 Antarctica, The Cryosphere, 11, 1797–1811, <https://doi.org/10.5194/tc-11-1797-2017>,
- 847 2017.
- 848 Grosvenor, D. P., Choularton, T. W., Lachlan-Cope, T., Gallagher, M. W., Crosier, J., Bower,
- 849 K. N., Ladkin, R. S., and Dorsey, J. R.: In-situ aircraft observations of ice concentrations
- 850 within clouds over the Antarctic Peninsula and Larsen Ice Shelf, Atmos. Chem. Phys., 12,
- 851 11275–11294, <https://doi.org/10.5194/acp-12-11275-2012>, 2012.
- 852 Hogan, R. J. and Illingworth, A. J.: The effect of specular reflection on spaceborne lidar
- 853 measurements of ice clouds, Report of the ESA Retrieval algorithm for EarthCARE project,
- 854 5 pp., 2003.
- 855 Kassianov E, Barnard J, Flynn C, Riihimaki L, Michalsky J, Hodges G (2014) Areal-averaged
- 856 spectral surface albedo from ground-based transmission data alone: toward an operational
- 857 retrieval. *Atmosphere* 5:597–621. <https://doi.org/10.3390/atmos503059>
- 858 King, J. C., Argentini, S. A., and Anderson, P. S.: Contrasts between the summertime surface
- 859 energy balance and boundary layer structure at Dome C and Halley stations, Antarctica, J.
- 860 Geophys. Res.-Atmos., 111, D02105, <https://doi.org/10.1029/2005JD006130>, 2006.

- 861 King, J. C., Gadian, A., Kirchgaessner, A., Kuipers Munneke, P., Lachlan-Cope, T. A., Orr, A.,
862 Reijmer, C., Broeke, M. R., van Wessem, J. M., and Weeks, M.: Validation of the
863 summertime surface energy budget of Larsen C Ice Shelf (Antarctica) as represented in
864 three high-resolution atmospheric models, *J. Geophys. Res.-Atmos.*, 120, 1335–1347,
865 <https://doi.org/10.1002/2014JD022604>, 2015.
- 866 Kratz, D. P., Gupta, S. K., Wilber, A. C., and Sothcott, V. E.: Validation of the CERES Edition-
867 4A Surface-Only Flux Algorithms, *J. Appl. Meteorol. Clim.*, 59, 281–295,
868 <https://doi.org/10.1175/JAMC-D-19-0068.1>, 2020.
- 869 Lachlan-Cope, T.: Antarctic clouds, *Polar Res.*, 29, 150–158, 2010.
- 870 Lachlan-Cope, T., Listowski, C., and O’Shea, S.: The microphysics of clouds over the Antarctic
871 Peninsula – Part 1: Observations, *Atmos. Chem. Phys.*, 16, 15605–15617,
872 <https://doi.org/10.5194/acp-16-15605-2016>, 2016.
- 873 Lamb, D., and J. Verlinde: Physics and chemistry of clouds. Cambridge University Press, 2011.
- 874 Lanconelli, C., Busetto, M., Dutton, E. G., König-Langlo, G., Maturilli, M., Sieger, R., Vitale,
875 V., and Yamanouchi, T.: Polar baseline surface radiation measurements during the
876 International Polar Year 2007–2009, *Earth Syst. Sci. Data*, 3, 1–8,
877 <https://doi.org/10.5194/essd-3-1-2011>, 2011.
- 878 Lawson, R. P. and Gettelman, A.: Impact of Antarctic mixed-phase clouds on climate, *P. Natl.
879 Acad. Sci. USA*, 111, 18156–18161, 2014.
- 880 Legrand, M., Yang, X., Preunkert, S., and Therys, N.: Year-round records of sea salt, gaseous,
881 and particulate inorganic bromine in the atmospheric boundary layer at coastal (Dumont
882 d’Urville) and central (Concordia) East Antarctic sites, *J. Geophys. Res. Atmos.*, 121, 997–
883 1023, <https://doi.org/10.1002/2015JD024066>, 2016.
- 884 Lemus, L., Rikus, L., Martin, C., and Platt, R.: Global cloud liquid water path simulations. *J.
885 Climate*, 10(1), 52–64, 1997.

- 886 Lenaerts, J. T., Van Tricht, K., Lhermitte, S. and L'Ecuyer, T. S.: Polar clouds and radiation in
887 satellite observations, reanalyses, and climate models, *Geophysical Research Letters*, 44(7),
888 3355-3364, 2017.
- 889 Listowski, C. and Lachlan-Cope, T.: The microphysics of clouds over the Antarctic Peninsula
890 – Part 2: modelling aspects within Polar WRF, *Atmos. Chem. Phys.*, 17, 10195–10221,
891 <https://doi.org/10.5194/acp-17-10195-2017>, 2017.
- 892 Listowski, C., Delanoë, J., Kirchgaessner, A., Lachlan-Cope, T., and King, J.: Antarctic clouds,
893 supercooled liquid water and mixed phase, investigated with DARDAR: geographical and
894 seasonal variations, *Atmos. Chem. Phys.*, 19, 6771–6808, <https://doi.org/10.5194/acp-19-6771-2019>, 2019.
- 895 Lubin, D., Chen, B., Bromwich, D. H., Somerville, R. C., Lee, W. H., and Hines, K. M.: The
896 Impact of Antarctic Cloud Radiative Properties on a GCM Climate Simulation, *J. Climate*,
897 11, 447-462, 1998.
- 898 Mishchenko, M. I., Hovenier, J. W., and Travis, L. D. (Eds.): *Light Scattering by Nonspherical
899 Particles: Theory, Measurements, and Applications*, Academic Press, chap. 14, 393–416,
900 2000.
- 901 Ohmura, A., Dutton, E. G., Forgan, B., Fröhlich, C., Gilgen, H., Hegner, H., Heimo, A., König-
902 Langlo, G., McArthur, B., Müller, G., Philipona, R., Pinker, R., Whitlock, C. H., Dehne,
903 K., and Wild, M.: Baseline Surface Radiation Network (BSRN/WCRP): New precision
904 radiometry for climate research, *B. Am. Meteorol. Soc.*, 79(10), 2115-2136, 1998.
- 905 O'Shea, S. J., Choularton, T. W., Flynn, M., Bower, K. N., Gallagher, M., Crosier, J., Williams,
906 P., Crawford, I., Flem- ing, Z. L., Listowski, C., Kirchgaessner, A., Ladkin, R. S., and
907 Lachlan-Cope, T.: In situ measurements of cloud microphysics and aerosol over coastal
908 Antarctica during the MAC campaign, *Atmos. Chem. Phys.*, 17, 13049–13070,
909 <https://doi.org/10.5194/acp-17-13049-2017>, 2017.

- 911 Pailleux, J., Geleyn, J.-F., El Khatib, R., Fischer, C., Hamrud, M., Thépaut, J.-N., Rabier, F.,
912 Andersson, E., Salmond, D., Burridge, D., Simmons, A., and Courtier, P.: Les 25 ans du
913 système de prévision numérique du temps IFS/Arpège, La Météorologie, 89, 18–27,
914 <https://doi.org/10.4267/2042/56594>, 2015.
- 915 Ricaud, P., Gabard, B., Derrien, S., Chaboureau, J.-P., Rose, T., Mombauer, A. and Czekala,
916 H.: HAMSTRAD-Tropo, A 183-GHz Radiometer Dedicated to Sound Tropospheric Water
917 Vapor Over Concordia Station, Antarctica, IEEE T. Geosci. Remote, 48, 1365–1380, doi:
918 [10.1109/TGRS.2009.2029345](https://doi.org/10.1109/TGRS.2009.2029345), 2010a.
- 919 Ricaud, P., Gabard, B., Derrien, S., Attié, J.-L., Rose, T., and Czekala, H.: Validation of
920 tropospheric water vapor as measured by the 183-GHz HAMSTRAD Radiometer over the
921 Pyrenees Mountains, France, IEEE T. Geosci. Remote, 48, 2189–2203, 2010b.
- 922 Ricaud, P., Genthon, C., Durand, P., Attié, J.-L., Carminati, F., Canut, G., Vanacker, J.-F.,
923 Moggio, L., Courcoux, Y., Pellegrini, A., and Rose, T.: Summer to Winter Diurnal
924 Variabilities of Temperature and Water Vapor in the lowermost troposphere as observed by
925 the HAMSTRAD Radiometer over Dome C, Antarctica, Bound.-Lay. Meteorol., 143, 227–
926 259, doi:10.1007/s10546-011-9673-6, 2012.
- 927 Ricaud, P., Grigioni, P., Zbinden, R., Attié, J.-L., Genoni, L., Galeandro, A., Moggio, A.,
928 Montaguti, S., Petenko, I., and Legovini, P.: Review of tropospheric temperature, absolute
929 humidity and integrated water vapour from the HAMSTRAD radiometer installed at Dome
930 C, Antarctica, 2009–14, Antarct. Sci., 27, 598–616, doi:10.1017/S0954102015000334,
931 2015.
- 932 Ricaud, P., Bazile, E., del Guasta, M., Lanconelli, C., Grigioni, P., and Mahjoub, A.: Genesis
933 of diamond dust, ice fog and thick cloud episodes observed and modelled above Dome C,
934 Antarctica, Atmos. Chem. Phys., 17, 5221–5237, <https://doi.org/10.5194/acp-17-5221-2017>, 2017.

- 936 Ricaud, P., Del Guasta, M., Bazile, E., Azouz, N., Lupi, A., Durand, P., Attié, J.-L., Veron, D.,
937 Guidard, V., and Grigioni, P.: Supercooled liquid water cloud observed, analysed, and
938 modelled at the top of the planetary boundary layer above Dome C, Antarctica, *Atmos.*
939 *Chem. Phys.*, 20, 4167–4191, <https://doi.org/10.5194/acp-20-4167-2020>, 2020.
- 940 Sippola, H., and Taskinen, P.: Activity of supercooled water on the ice curve and other
941 thermodynamic properties of liquid water up to the boiling point at standard pressure, *J.*
942 *Chem. Engineer. Data*, 63(8), 2986-2998, 2018.
- 943 Storelvmo, T. and Tan, I.: The Wegener–Bergeron–Findeisen process—Its discovery and vital
944 importance for weather and climate, *Meteor. Z.*, 24, 455-461, 2015.
- 945 Stull, R. B.: An introduction to boundary layer meteorology, Kluwer Academic Publisher,
946 1988.
- 947 Tomasi, C., Petkov, B., Mazzola, M., Ritter, C., di Sarra, A., di Iorio, T., and del Guasta, M.:
948 Seasonal variations of the relative optical air mass function for background aerosol and thin
949 cirrus clouds at Arctic and Antarctic sites, *Remote Sensing*, 7(6), 7157-7180, 2015.
- 950 Wegener, A. 1911. Thermodynamik der Atmosphäre. – Leipzig, Germany: Barth.
- 951 Wille, J. D., Favier, V., Dufour, A., Gorodetskaya, I. V., Turner, J., Agosta, C. and Codron, F.:
952 West Antarctic surface melt triggered by atmospheric rivers, *Nature Geoscience*, 12(11),
953 911-916, 2019.
- 954 Young, G., Lachlan-Cope, T., O’Shea, S. J., Dearden, C., Listowski, C., Bower, K. N.,
955 Choularton, T. W., and Gallagher, M. W.: Radiative effects of secondary ice enhancement
956 in coastal Antarctic clouds, *Geophys. Res. Lett.*, 46, 2312–2321,
957 <https://doi.org/10.1029/2018GL080551>, 2019.
- 958

959

Tables

960 **Table 1.** Cloud-free periods in December 2018-2021 detected from the LIDAR depolarization*
 961 observations at Concordia. Time is in UTC. MM-NN means from MM (included) hour UTC to
 962 NN (excluded) hour UTC. “X” means no cloud-free period during that day. “ND” means no
 963 LIDAR data available. Greyish cases mean that cloud-free irradiance calculations are
 964 impossible due to lack of some data (LIDAR, HAMSTRAD, BSRN or AWS).

Mis en forme : Surlignage
Mis en forme : Interligne : Double
Mis en forme : Surlignage

Mis en forme : Surlignage

Days	2018	2019	2020	2021
01	0-24	9-18	ND	9-16
02	0-21	13-17	ND	7-8
03	0-24	6-16	ND	6-24
04	X	11-16	ND	0-24
05	X	6-16	3-16	12-19
06	3-6	0-13	9-13	2-12
07	1-16	X	X	0-24
08	3-15	X	1-2	0-10
09	2-16	X	4-14	10-17
10	0-3	X	X	ND
11	X	4-17	0-1	ND
12	X	X	20-22	ND
13	11-13	10-14	0-12	X
14	22-24	17-18	X	5-12 & 17-20
15	4-8	22-23	X	3-6
16	15-18	X	6-8	11-24
17	18-19	ND	X	0-24
18	1-17	ND	16-17	0-3
19	0-24	ND	7-9 & 11-13	20-23
20	0-12	ND	20-22	16-19
21	X	ND	20-21	X
22	9-16	ND	ND	12-15
23	1-4	ND	14-20	X
24	X	ND	11-14	0-6
25	X	ND	9-15	20-24
26	12-18	ND	0-16 & 18-22	0-24
27	10-11	ND	0-2	0-4
28	0-6	ND	0-17	10-14
29	X	ND	0-18	X
30	X	ND	7-24	X
31	10-12	ND	0-18	X

965

966 **Table 1.** Time-coincident data availability (green) in Decembers 2018–2021 for HAMSTRAD
967 temperature and LWP, Lidar Backscattering and Depolarization and BSRN Surface Radiances
968 (Net, LWD, LWU, SWD and SWU). The 5 clear-sky (Reference) days are highlighted in red.

Year	December Days																														
	1	2	3	4	5	6	7	8	9	10	11	12	13	14	15	16	17	18	19	20	21	22	23	24	25	26	27	28	29	30	31
2018																															
2019																															
2020																															
2021																															

969
970

971

Table 2. Gaussian functions fitted to the $N(x)$ function for $x = T$ (°C) or ΔF (W m⁻²). Units of

973 a_1, a_2, a_3 , and c_0 are in count number for T and ΔF ; units of $\mu_1, \mu_2, \mu_3, \sigma_1, \sigma_2$, and σ_3 are in

974 $^{\circ}\text{C}$ for T and in W m^{-2} for ΔF .

Σ	a_1	μ_1	σ_1	a_2	μ_2	σ_2	a_3	μ_3	σ_3	c_0
T	<u>15.0</u> 10^3	<u>-31.5</u>	<u>1.45</u>	<u>5.0</u> 10^3	<u>-28.0</u>	<u>1.65</u>	<u>0.5</u> 10^3	<u>-19.0</u>	<u>2.5</u>	<u>-9.1</u> 10^{-6}
ΔF_{net}	<u>371.7</u>	<u>10.0</u>	<u>11.5</u>	<u>74.6</u>	<u>37.6</u>	<u>21.1</u>	<u>220.8</u>	<u>57.5</u>	<u>14.1</u>	<u>-10.2</u>
ΔF_{LW}^{Down}	<u>415.5</u>	<u>10.0</u>	<u>10.4</u>	<u>189.5</u>	<u>53.7</u>	<u>24.2</u>	<u>227.1</u>	<u>82.9</u>	<u>7.0</u>	<u>-18.5</u>
ΔF_{LW}^{Up}	<u>z</u>	<u>z</u>	<u>z</u>	<u>z</u>	<u>z</u>	<u>z</u>	<u>z</u>	<u>z</u>	<u>z</u>	<u>z</u>
ΔF_{SW}^{Down}	<u>190.5</u>	<u>-10.1</u>	<u>17.2</u>	<u>113.0</u>	<u>-80.0</u>	<u>54.6</u>	<u>z</u>	<u>z</u>	<u>z</u>	<u>-1.9</u>
ΔF_{SW}^{Up}	<u>282.4</u>	<u>-10.1</u>	<u>12.8</u>	<u>133.8</u>	<u>-75.0</u>	<u>41.8</u>	<u>z</u>	<u>z</u>	<u>z</u>	<u>8.3</u>

975

Table 2. Gaussian functions fitted to the $N(x)$ function for $x = \theta$ ($^{\circ}\text{C}$) or ΔSR (W m^{-2}). Units

977 of a_1 , a_2 , a_3 , and c are in count number for θ and ΔSR ; units of μ_1 , μ_2 , μ_3 , σ_1 , σ_2 , and σ_3 are
978 in $^{\circ}\text{C}$ for θ and in W m^{-2} for ΔSR .

x	a_x	μ_x	σ_x	a_z	μ_z	σ_z	a_3	μ_3	σ_3	ϵ
θ	$15.0 \cdot 10^3$	-31.5	1.45	$5.0 \cdot 10^3$	-28.0	1.65	$0.5 \cdot 10^3$	-19.0	2.5	$-9.1 \cdot 10^{-6}$
Net ASR	2106.5	0.02	19.2	941.4	29.8	22.0	-	-	-	19.5
LWD ASR	1010.8	80.1	21.9	1565.6	10.0	23.9	-	-	-	18.4
LWU ASR	1476.4	-10.0	14.9	1834.7	25.0	16.2	-	-	-	185.4
SWD ASR	1317.2	-5.0	15.8	717.4	-80.0	64.7	-	-	-	9.1
SWU ASR	1928.8	-5.0	19.2	1163.4	-59.9	17.6	-	-	-	9.1

981 **Table 3.** Coefficients of the relations $f(LWP) = \alpha + \beta \ln(LWP)$ for the temperature T or
 982 cloud radiative forcing components ΔF . Units of T and ΔF , as well as of their corresponding
 983 “ α ” values are in $^{\circ}\text{C}$ and W m^{-2} , respectively; units of β are in $^{\circ}\text{C g}^{-1} \text{m}^2$ for T and in W g^{-1} for
 984 ΔF ; units of LWP are in g m^{-2} . The last column shows the range of LWP values for which the
 985 relation is valid. $\alpha \pm \delta\alpha$ corresponds to the range of α values where the relationship is valid.

$f(LWP)$	$\alpha \pm \delta\alpha$	β	Valid range for T or ΔF	Valid range for LWP
T	-33.8 ± 1.5	6.5	[−36; −16]	[1.0; 14.0]
ΔF_{net}	-18.0 ± 10.0	70.0	[0; 70]	[1.2; 3.5]
ΔF_{LW}^{Down}	5.0 ± 15.0	65.0	[0; 90]	[1.0; 3.5]
ΔF_{LW}^{Up}	0 ± 5.0	0.0	[−5; 5]	[0.0; 6.5]
ΔF_{SW}^{Down}	30.0 ± 30.0	-130.0	[−130; 0]	[1.5; 4.0]
ΔF_{SW}^{Up}	30.0 ± 30.0	-110.0	[−110; 00]	[1.5; 4.0]

987 **Table 3.** Coefficients of the relations $f(LWP) = a + b \ln(LWP)$ for the temperature θ or
 988 surface radiation anomalies ΔSR . Units of θ and ΔSR , as well as of their corresponding “ a ”
 989 values are in $^{\circ}\text{C}$ and W m^{-2} , respectively; units of b are in $^{\circ}\text{C g}^{-1} \text{m}^2$ for θ and in W g^{-1} for ΔSR ;
 990 units of LWP are in g m^{-2} . The last column shows the range of LWP values for which the
 991 relation is valid (in black), and in red (blue) the sub range in which a positive (negative) impact
 992 is observed on ΔSR . Note that $a \pm \delta a$ corresponds to the range of a values where the
 993 relationship is valid.

$f(LWP)$	$a \pm \delta a$	b	Valid range for θ or ΔSR	Valid range for LWP
θ	-33.8 ± 1.5	6.5	[−36; −16]	[1.0; 14.0]
Net ΔSR	-50.0 ± 10.0	90.0	[−15; 50]	[1.5; 3.0] / [1.7; 3.0]

LWDΔSR	5.0 ± 15.0	65.0	$[-10; 100]$	[0.8; 4.0]/[1.0; 4.0]
LWUΔSR	-45.0 ± 30.0	90.0	$[-20; 40]$	[1.3; 2.5]/[1.6; 2.5]
SWDΔSR	30.0 ± 30.0	-130.0	$[-140; 10]$	[1.1; 3.8]/[1.2; 3.8]
SWUΔSR	15.0 ± 15.0	-75.0	$[-75; 10]$	[1.1; 3.2]/[1.2; 3.2]

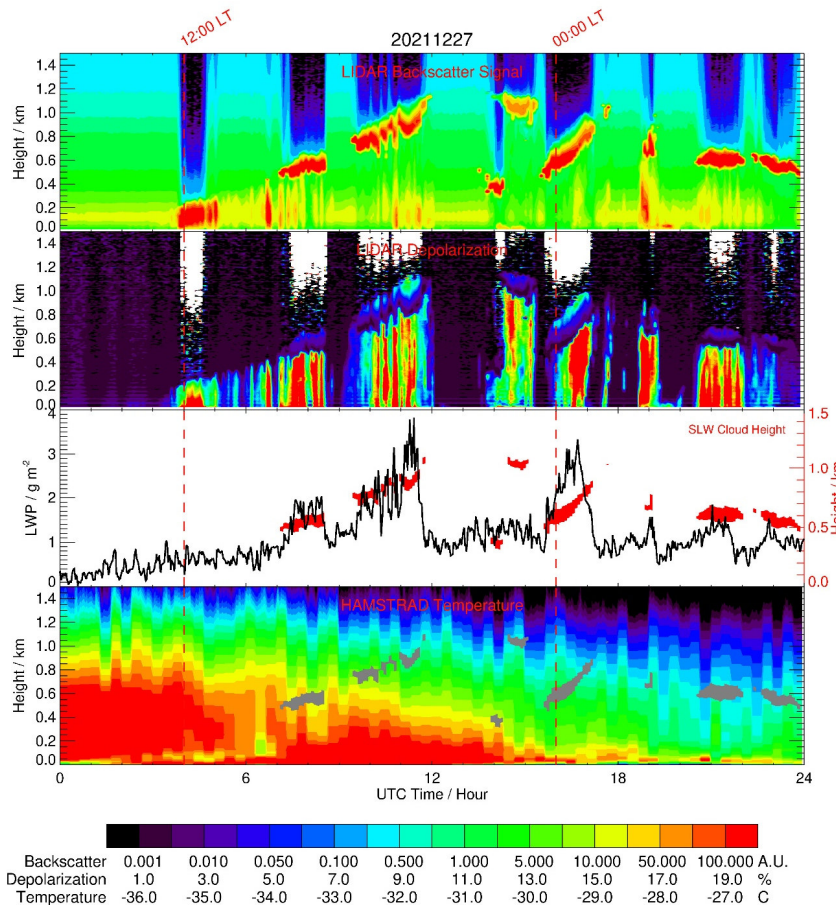
994
995

996

997

998

Figures

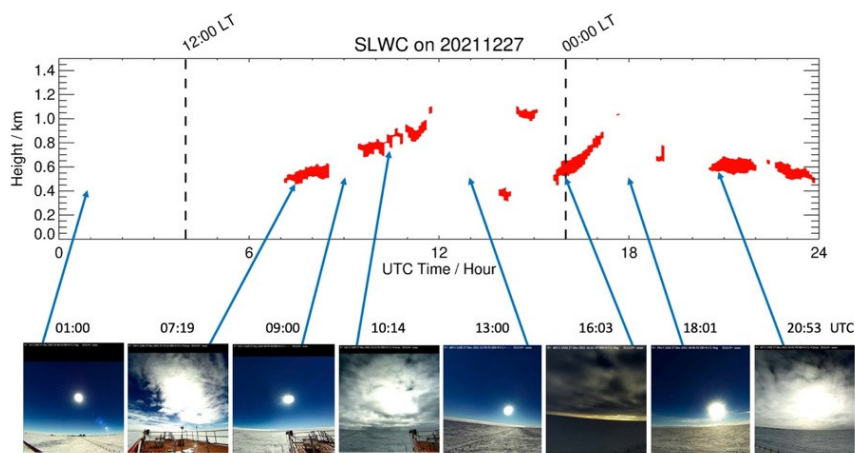


999

1000 **Figure 1:** (From top to bottom): Time evolution (UTC, hour) of the LIDAR backscattering
 1001 signal, the Lidar depolarization signal, the HAMSTRAD
 1002 LWP and the HAMSTRAD temperature profile measured on 27 December 2021. The time
 1003 evolution of the SLW cloud (as diagnosed by a backscattering signal_value > 60 A.U. and a
 1004 depolarization signal_value < 5%) is highlighted by the red and grey areas in the third and the
 1005 forth panel from the top, respectively. The height above the ground is shown on the third panel

Mis en forme : Surlignage

1006 from the top with the y-axis on the right. The 00:00 and 12:00 local times (LT) are highlighted
1007 by 2 vertical dashed lines.



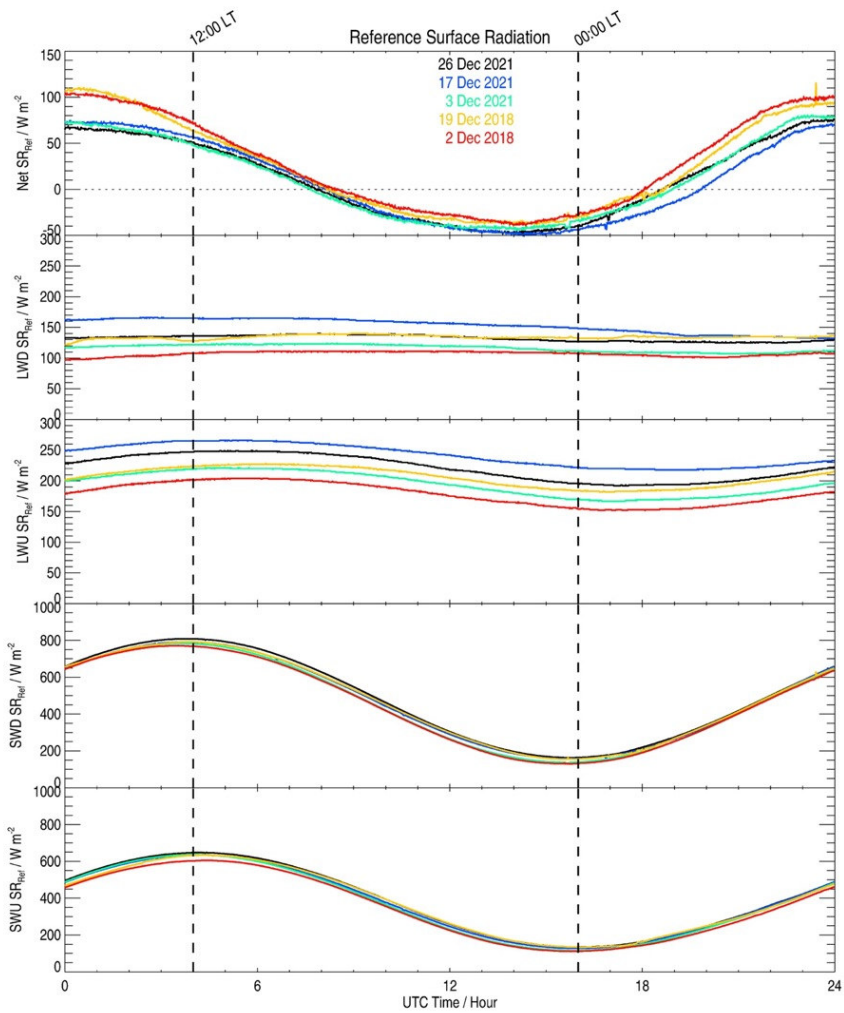
1008

1009 **Figure 2:** (Top) Time evolution (UTC, hour) of the SLWC (red areas) on 27 December 2021.

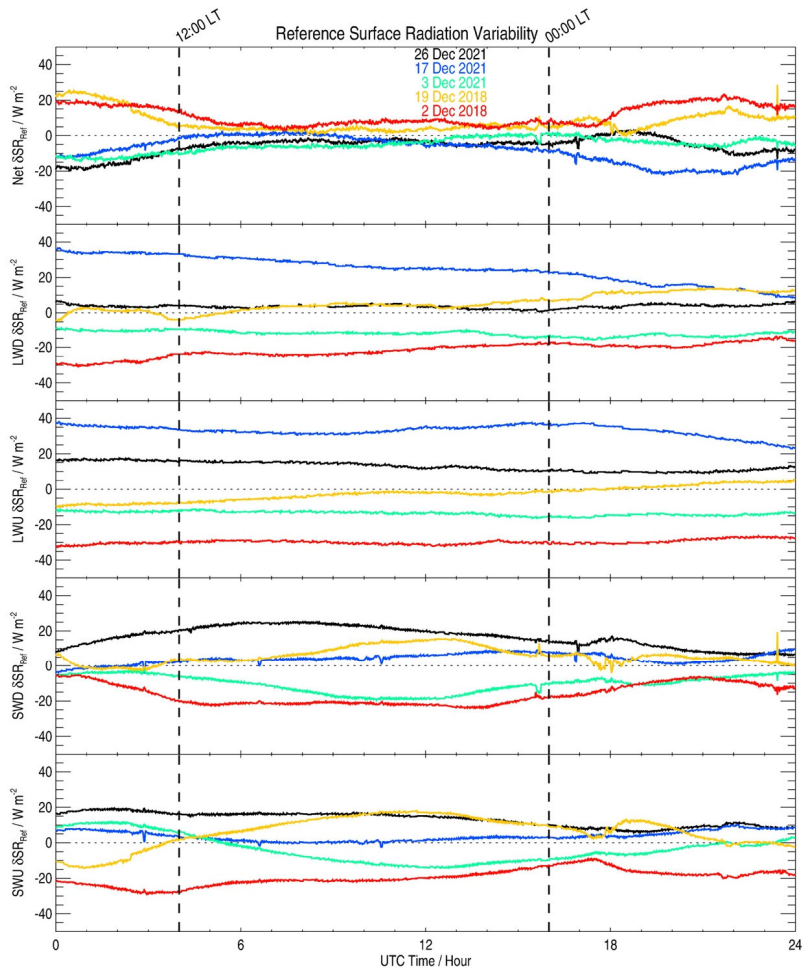
1010 (Bottom, from left to right) Snapshots from the HALO-CAM video camera taken on: 01:00 (no
 1011 SLWC), 07:19 (SLWC), 09:00 (no SLWC), 10:14 (SLWC), 13:00 (no SLWC), 16:03 (SLWC),
 1012 18:01 (no SLWC) and 20:53 UTC (SLWC). The 00:00 and 12:00 local times (LT) are
 1013 highlighted by 2 vertical dashed lines.

1014

1015



1016
1017 **Figure 3:** Time evolution (UTC, hour) of the clear-sky surface radiations (SR, W m^{-2}) observed
1018 by the BSRN instruments on 2 December 2018 (red), 19 December 2018 (orange), 3 December
1019 2021 (green), 17 December 2021 (blue) and 26 December 2021 (black). (from top to bottom)
1020 Net SR, Longwave Downward SR (LWD SR), Longwave Upward SR (LWU SR), Shortwave
1021 Downward SR (SWD SR) and Shortwave Upward SR (SWU SR). The 00:00 and 12:00 local
1022 times (LT) are highlighted by 2 vertical dashed lines.



1023
1024
1025
1026
1027
1028

Figure 4: Time evolution (UTC, hour) of the clear-sky surface radiation variability ($\delta\text{SR}_{\text{Ref}}$, W m⁻²), namely the clear-sky surface radiations observed by the BSRN instruments on 2 December 2018 (red), 19 December 2018 (orange), 3 December 2021 (green), 17 December 2021 (blue) and 26 December 2021 (black) minus the corresponding values averaged over the 5 cloud-free days: (from top to bottom) Net SR, Longwave Downward SR (LWD SR), Longwave Upward

1029 SR (LWU SR), Shortwave Downward SR (SWD SR) and Shortwave Upward SR (SWU SR).

1030 The 00:00 and 12:00 local times (LT) are highlighted by 2 vertical dashed lines.

1031

1032

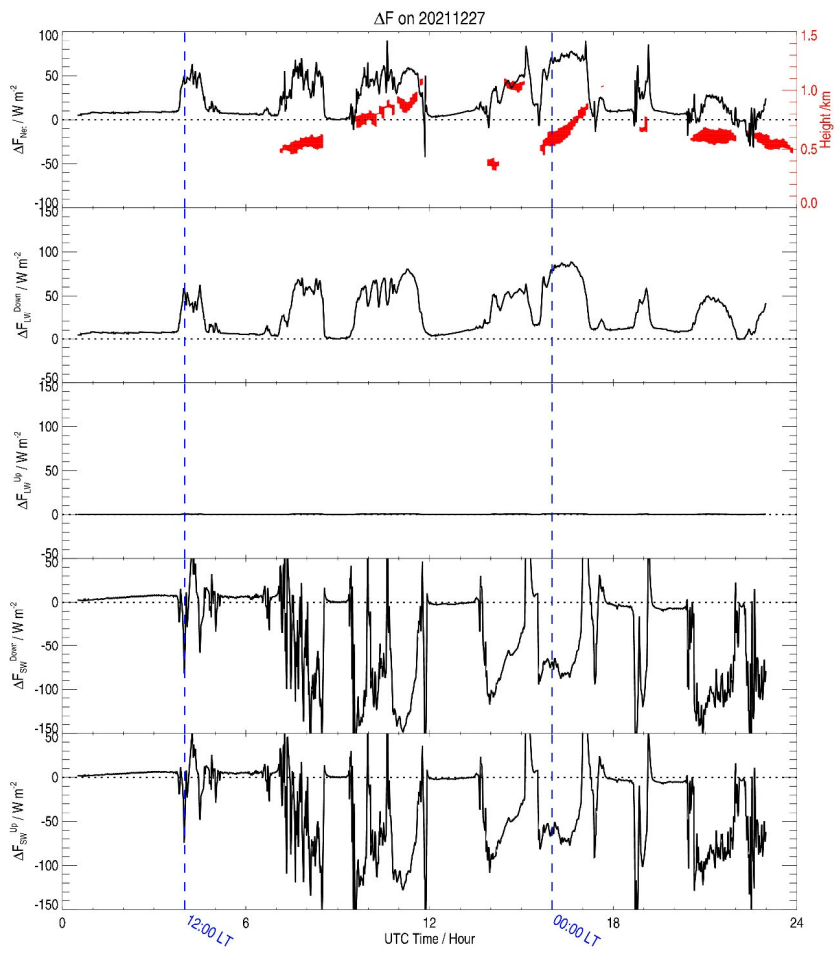
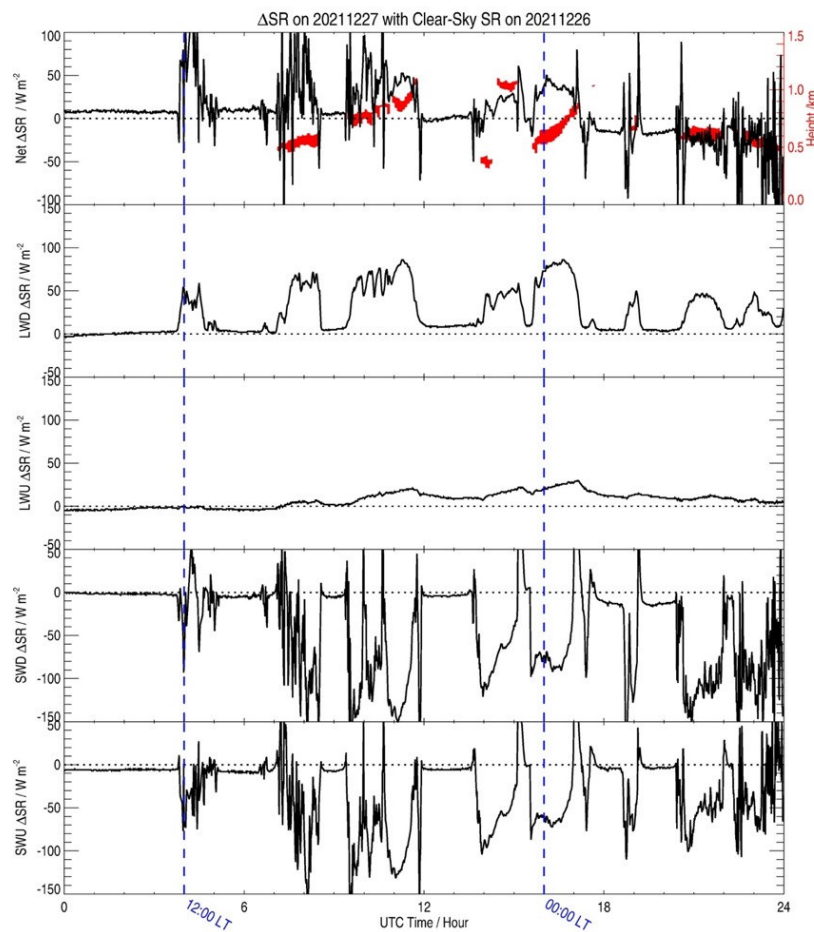


Figure 3: Time evolution (UTC, hour) of the cloud radiative forcing component (ΔF) (W m^{-2}) calculated on 27 December 2021: (from top to bottom) net (ΔF_{net}), longwave downward (ΔF_{LW}^{Down}), longwave upward (ΔF_{LW}^{Up}), shortwave downward (ΔF_{SW}^{Down}) and shortwave upward (ΔF_{SW}^{Up}). The SLW cloud layer (if present) is highlighted by a red area in the uppermost panel, with the height on the y-axis shown on the right. The 00:00 and 12:00 local times (LT) are highlighted by 2 vertical blue dashed lines.

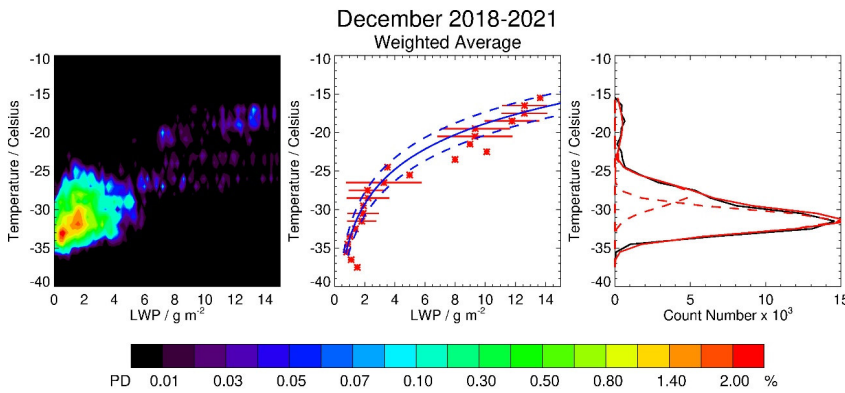
1040



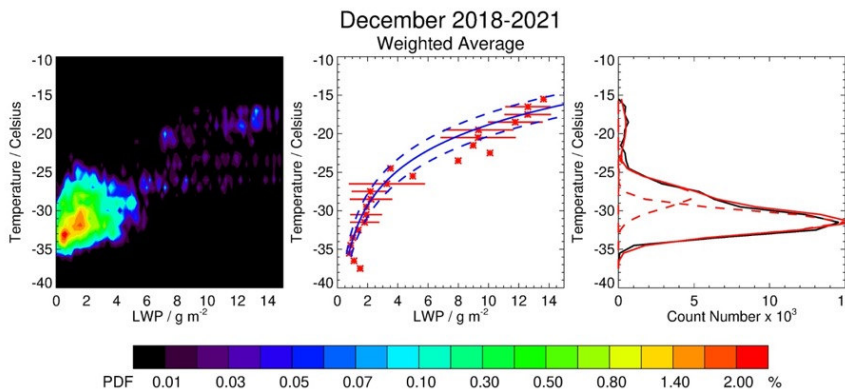
1041

1042 **Figure 5:** Time evolution (UTC, hour) of the Surface Radiation Anomaly (ΔSR), difference
 1043 between the SR ($W m^{-2}$) measured on 27 December 2021 and the reference clear-sky (SR_{ref})
 1044 SR ($W m^{-2}$) measured on 26 December 2021: (from top to bottom) Net (Net ΔSR), longwave
 1045 downward (LWD ΔSR), longwave upward (LWU ΔSR), shortwave downward (SWD ΔSR) and
 1046 shortwave upward (SWU ΔSR). The time evolution of the SLW cloud is highlighted by a red

1047 area in the uppermost panel, with the height on the y axis shown on the right. The 00:00 and
1048 12:00 local times (LT) are highlighted by 2 vertical blue dashed lines.



1049



1050
1051 **Figure 64:** (Left) Probability Density (PD, %) of the **Temperature ($^{\circ}\text{C}$)** as a function of Liquid
1052 Water Path (LWP, g m^{-2}) **contained** in the **Supercooled Liquid Water clouds (SLWCs)** **above**
1053 **Dome C** in December 2018-2021. The Probability Density is defined in the text. (Centre)
1054 Weighted-average LWP vs. temperature (red asterisks) with a fitted logarithmic function (blue
1055 solid) encompassing the significant points (**within the two** **2** **dashed blue lines**). Horizontal bars
1056 represent 1-sigma variability in LWP per 1 $^{\circ}\text{C}$ -wide bin **over significant points**. (Right)
1057 Temperature as a function of count number per 1 $^{\circ}\text{C}$ -wide bin (black solid line) **with** **3** **fitted**

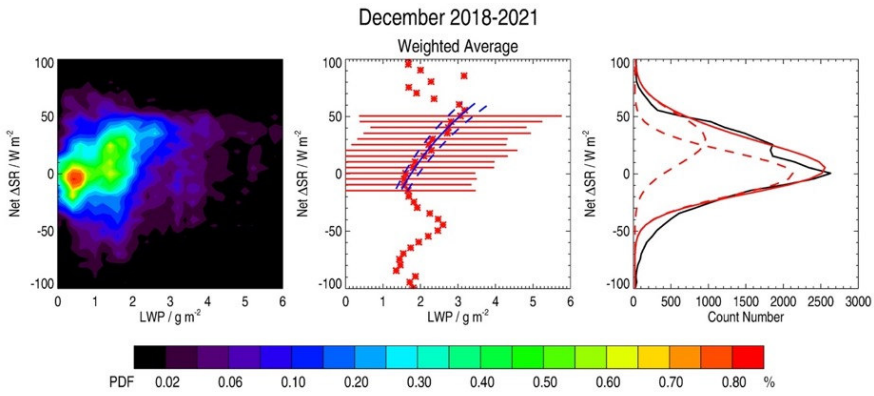
Mis en forme : Surlignage

1058 with three Gaussian functions (red dashed curves). The sum of the ~~three~~ Gaussian functions
1059 is represented by a red solid line.

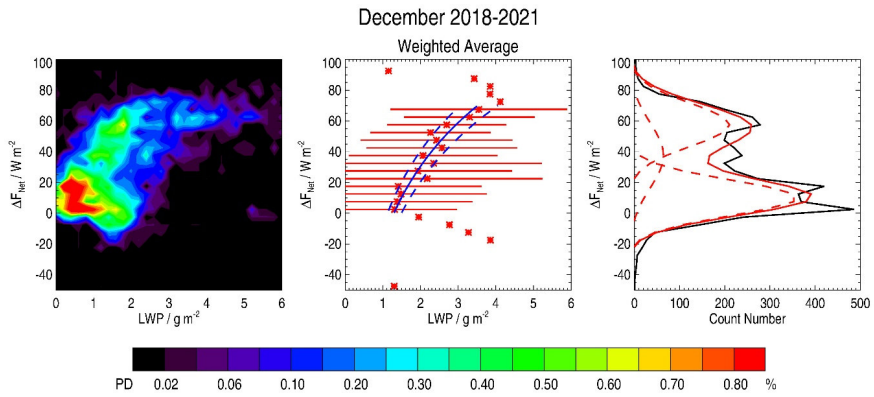
Mis en forme : Surlignage
Mis en forme : Surlignage

1060

1061



1062



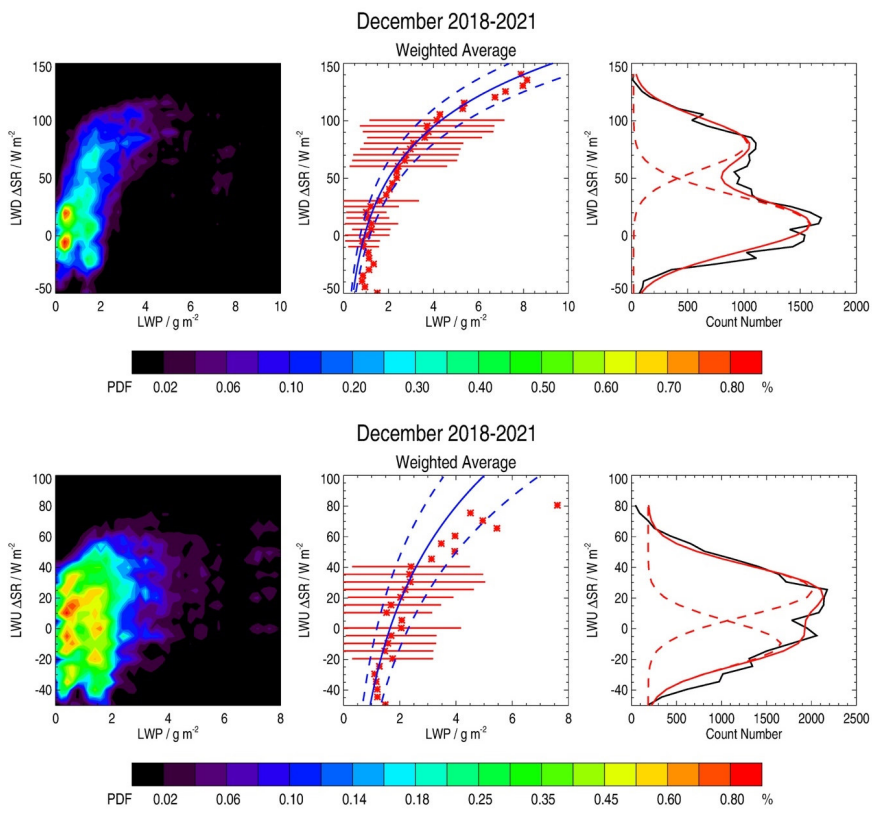
1063

Figure 5: (Left) Probability Density (PD, %) of the net cloud radiative forcing (ΔF_{net} , $W m^{-2}$) as a function of Liquid Water Path (LWP, $g m^{-2}$) in the SLWCs in December 2018-2021. The Probability Density is defined in the text. (Centre) Weighted-average LWP vs. ΔF_{net} with a fitted logarithmic function (blue solid) encompassing the significant points (within the two dashed blue lines). Horizontal bars represent 1-sigma variability in LWP per 5 $W m^{-2}$ -wide bin. (Right) ΔF_{net} as a function of count number per 5 $W m^{-2}$ -wide bin (black solid line) fitted with three Gaussian functions (red dashed curves). The sum of the three Gaussian functions is represented by a red solid line.

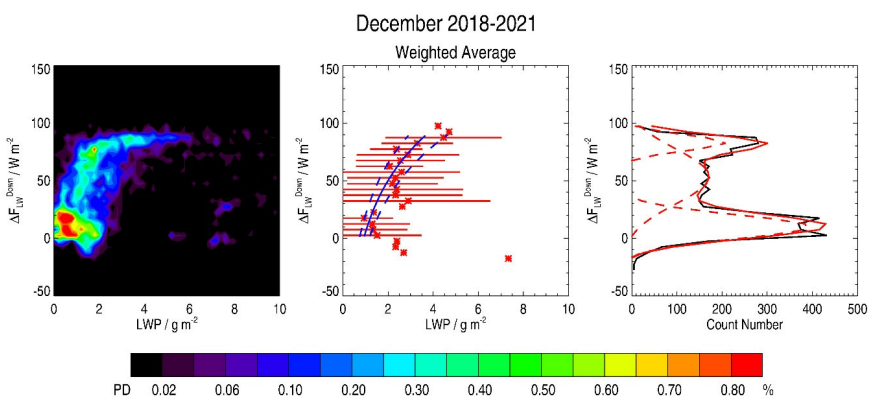
Mis en forme : Surlignage
 Mis en forme : Interligne : Double
 Mis en forme : Surlignage
 Mis en forme : Surlignage

1072 **Figure 7:** (Left) Probability Density (%) of the Net Surface Radiation Anomaly (Net ΔSR , W
1073 m^{-2}) as a function of Liquid Water Path (LWP, g m^{-2}) contained in the Supercooled Liquid
1074 Water clouds (SLWCs) above Dome C in December 2018-2021. The Probability Density is
1075 defined in the text. (Centre) Weighted average LWP vs. Net ΔSR (red asterisks) with a fitted
1076 logarithmic function (blue solid) encompassing the significant points (2 dashed blue lines).
1077 Horizontal bars represent 1 sigma variability in LWP per 5 W m^{-2} wide bin over significant
1078 points. (Right) Net ΔSR as a function of count number per 5 W m^{-2} wide bin (black solid line)
1079 with 2 fitted Gaussian functions (red dashed curves). The sum of the 2 Gaussian functions is
1080 represented by a red solid line.

1081



1082



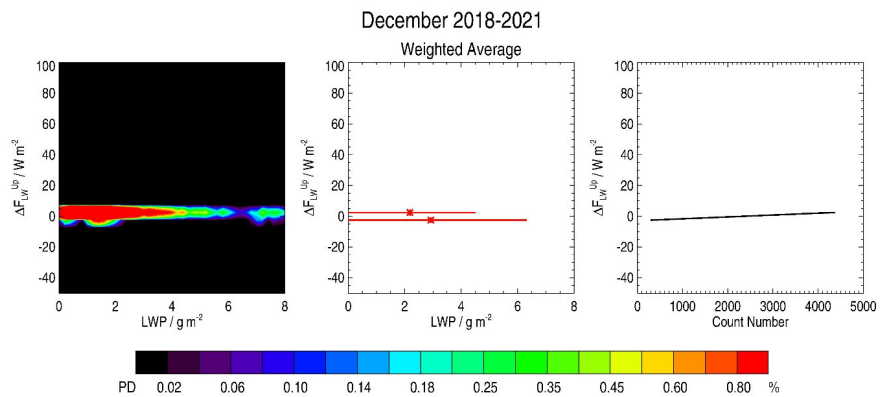
1083

1084 **Figure 6:** As in Figure 5 but for ΔF_{LW}^{Down} .

1085

- Mis en forme : Surlignage
- Mis en forme : Surlignage
- Mis en forme : Interligne : Double
- Mis en forme : Surlignage
- Mis en forme : Surlignage
- Mis en forme : Surlignage

1086



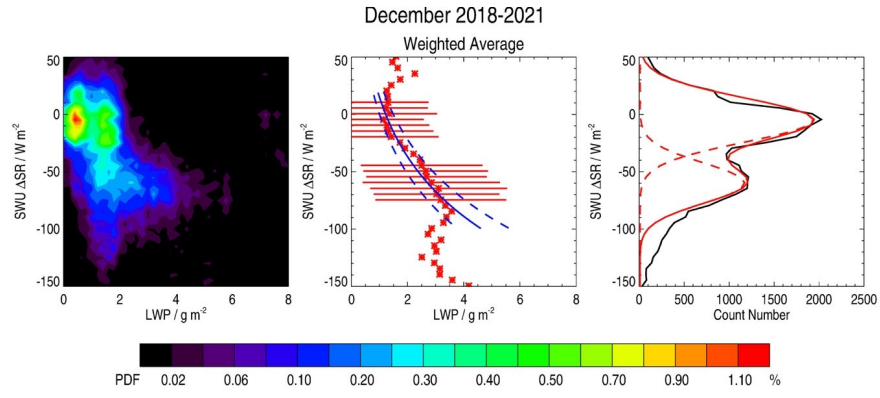
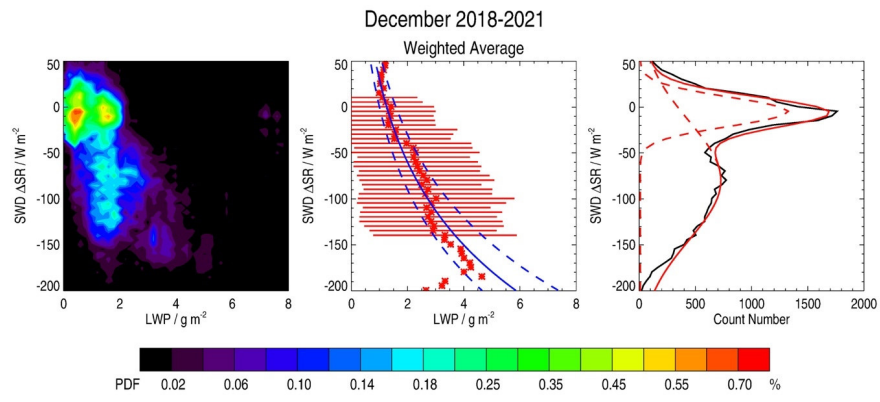
1087

1088 **Figure 78:** As in Figure 7-5 but for $\Delta F_{\text{LW}}^{\text{Up}}$
 1089 for the Longwave Downward (top) and Upward (bottom) Surface Radiation Anomaly (LWD
 1090 and LWU ΔSR , respectively).

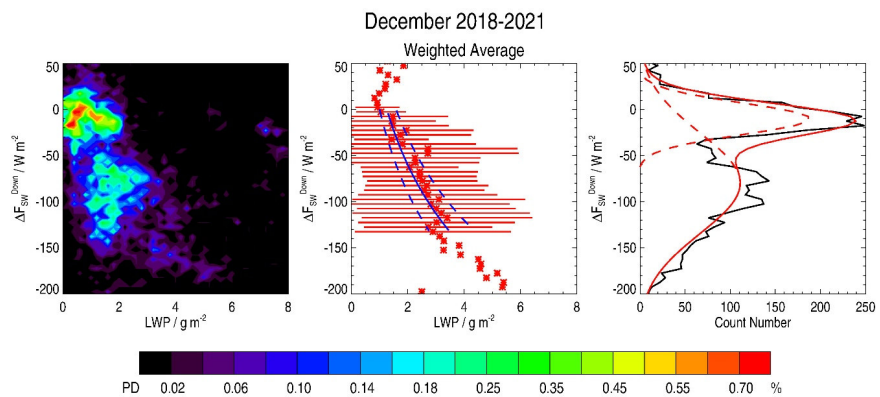
Mis en forme : Surlignage
 Mis en forme : Surlignage

1091

1092



1093

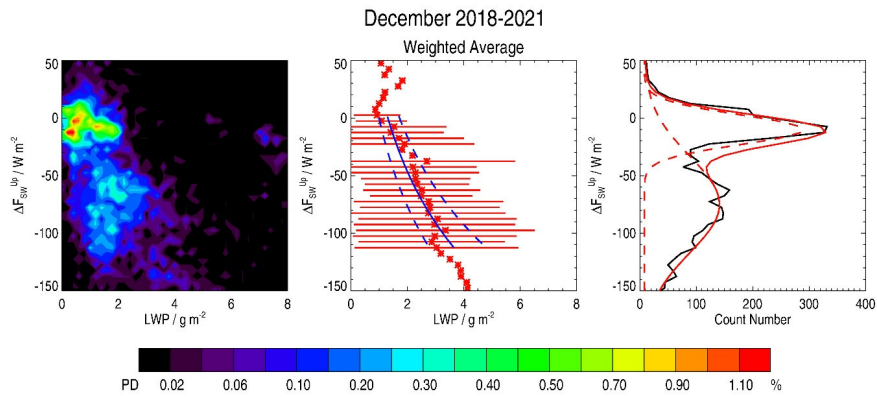


1094

1095 **Figure 8:** As in Figure 5 but for ΔF_{SW}^{Down} .

1096

Mis en forme : Surlignage
 Mis en forme : Surlignage



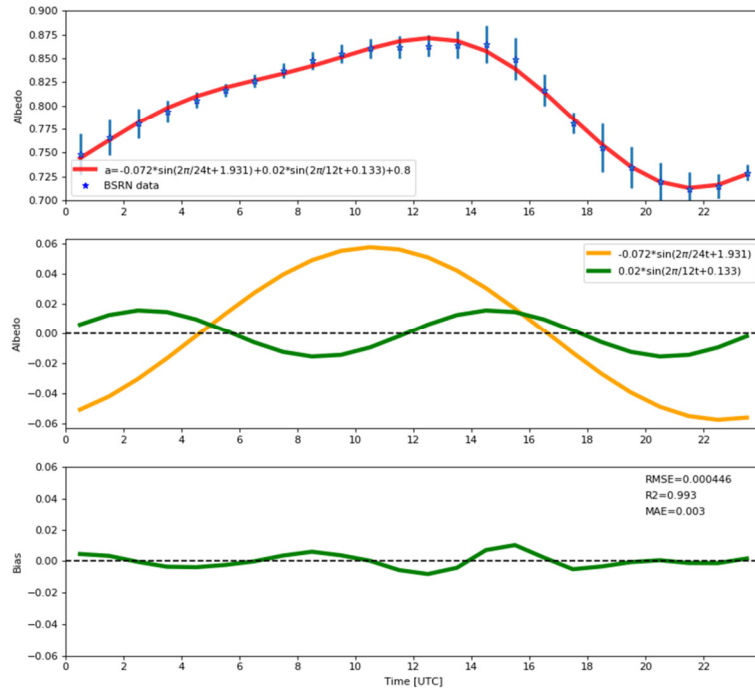
1097
1098 **Figure 99:** As in Figure 7-5 but for the Shortwave Downward (top) and ΔF_{SW}^{Up} Upward (bottom) Surface Radiation Anomaly (SWD and SWU ASR, respectively).
1099
1100
1101

Mis en forme : Surlignage
Mis en forme : Surlignage



1102
1103 **Figure 10:** Image of the sastrugi on the ice surface (Wikimedia Commons).
1104
1105
1106

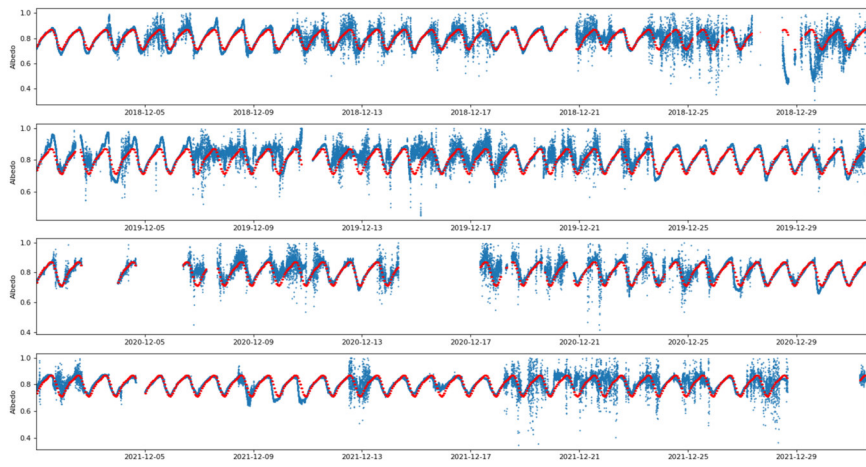
Mis en forme : Surlignage
Mis en forme : Gauche



1107
1108 **Figure 11:** (Top) Hourly time evolution (UTC, hour) of the mean surface albedo observed by
1109 the BSRN instruments and the associated standard deviation (blue star and vertical bar,
1110 respectively) for the 5 cloud-free periods under consideration in our analysis together with the
1111 fitted trigonometric function based on 2 sine functions (red line). (Centre) The 2 sine functions
1112 fitting the hourly time evolution of the BSRN mean surface albedo. (Bottom) Hourly time
1113 evolution (UTC, hour) of the albedo residuals (BSRN-fit, green line) and corresponding values
1114 of associated Root Mean Square Error (RMSE), Coefficient of determination (R^2), and Mean
1115 Absolute Error (MAE).

Mis en forme : Surlignage

Mis en forme : Gauche



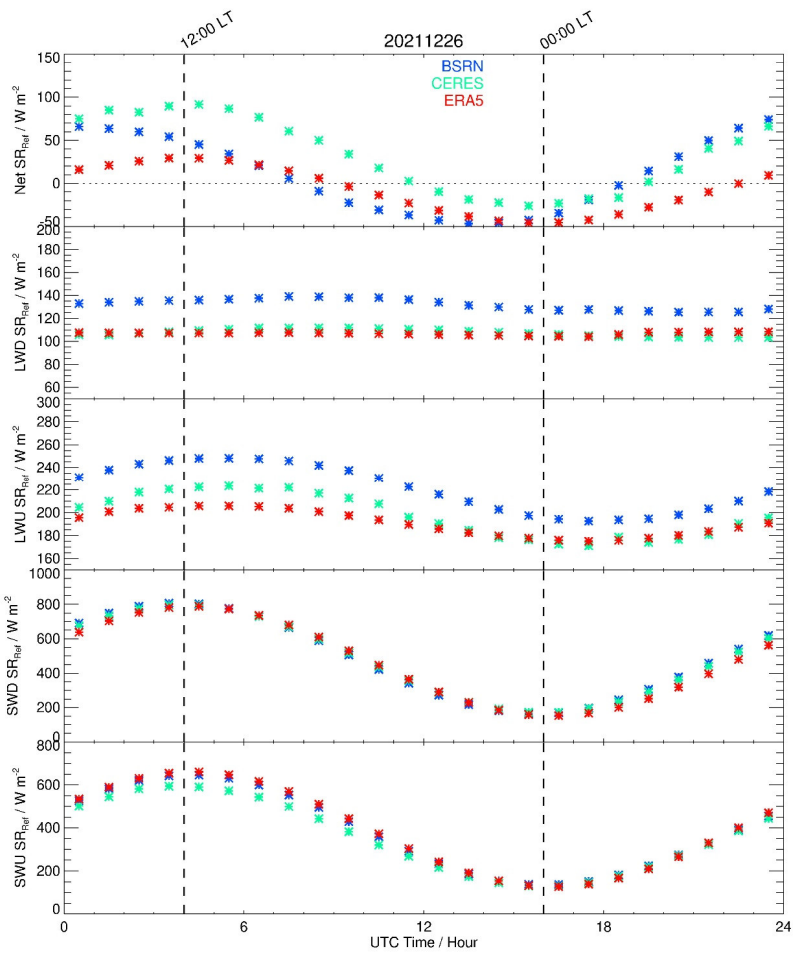
1117

1118 **Figure 12:** (from top to bottom) Hourly time evolution (UTC) of the surface albedo observed
 1119 by the BSRN instruments (blue), and using the fit based on 2 sine functions (red) for the whole
 1120 BSRN data set covering the month of December in: 2018, 2019, 2020 and 2021.

Mis en forme : Surlignage

Mis en forme : Surlignage

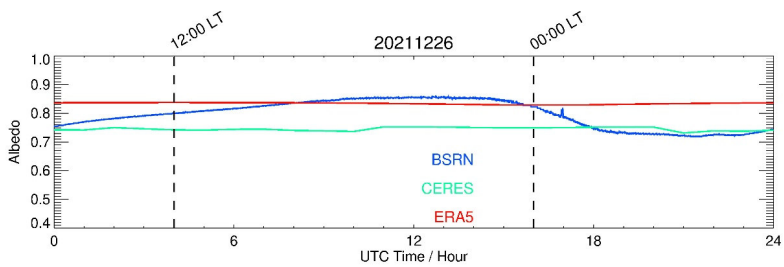
Mis en forme : Surlignage



1122

1123 **Figure 10:** Hourly time evolution (UTC, hour) of the clear-sky surface radiations (SR, W m^{-2})
 1124 observed by the BSRN instruments (blue asterisks), the CERES (green asterisks) and the ERA5
 1125 (red asterisks) data sets on 26 December 2021: (from top to bottom) Net SR, Longwave
 1126 Downward SR (LWD SR), Longwave Upward SR (LWU SR), Shortwave Downward SR
 1127 (SWD SR) and Shortwave Upward SR (SWU SR). The 00:00 and 12:00 local times (LT) are
 1128 highlighted by 2 vertical dashed lines.

1129



1130

1131 **Figure 11:** Time evolution (UTC, hour) of the surface albedo observed by the BSRN
 1132 instruments (blue), the CERES (green) and the ERA5 (red) data sets on 26 December 2021.
 1133 The 00:00 and 12:00 local times (LT) are highlighted by 2 vertical dashed lines.

1134

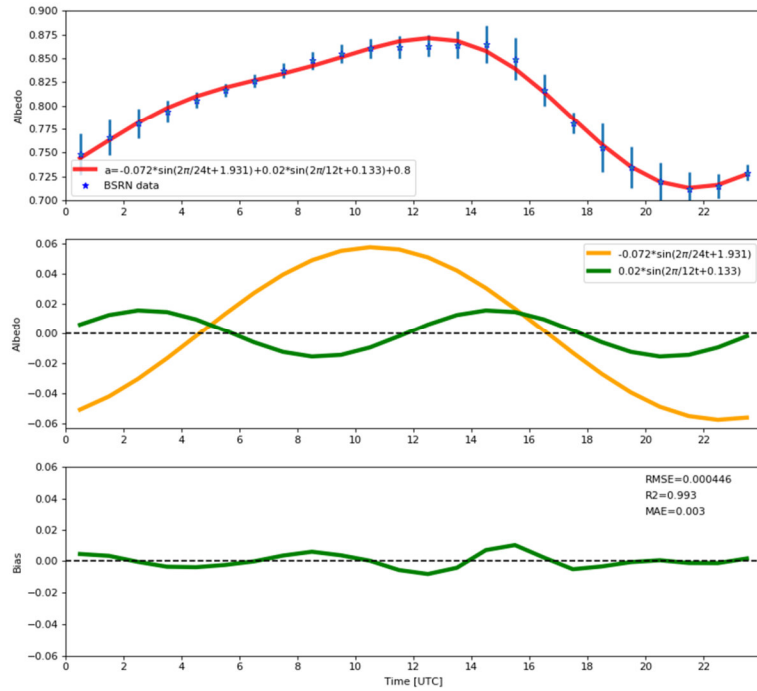
1135

← - - Mis en forme : Interligne : Double



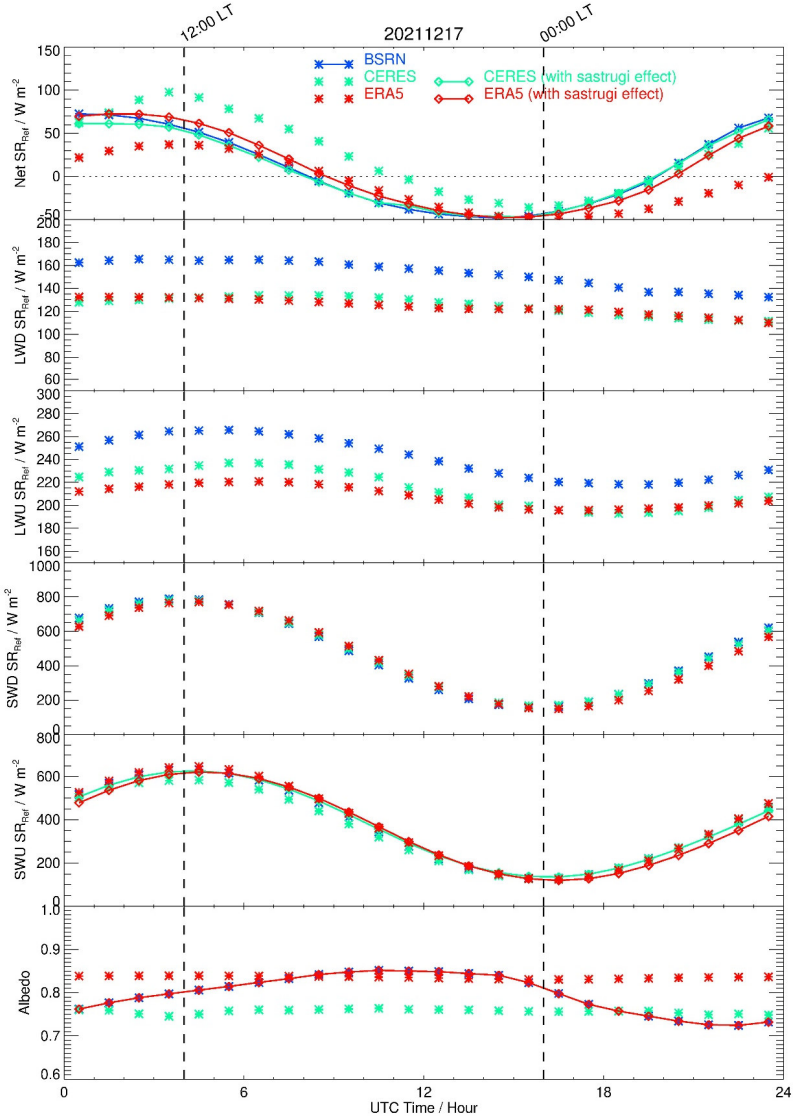
1136

1137 **Figure 12:** Image of the sastrugi on the ice surface (Wikimedia Commons).

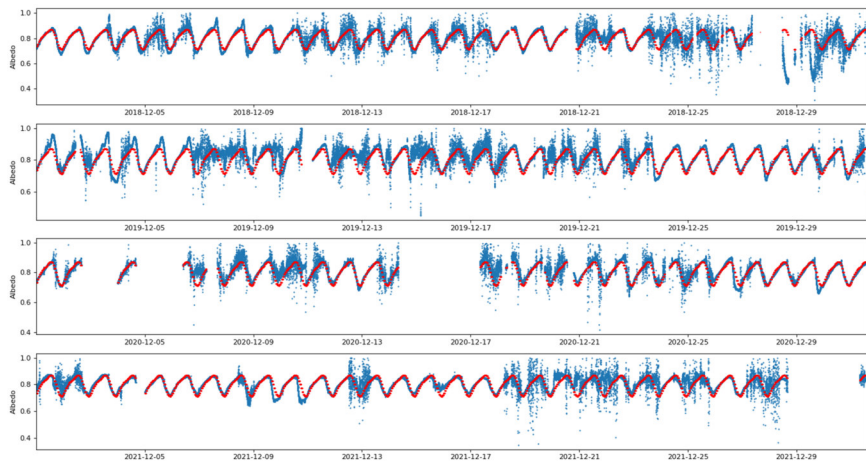


1138
1139 **Figure 13:** (Top) Hourly time evolution (UTC, hour) of the mean surface albedo observed by
1140 the BSRN instruments (blue star) associated with the 5 clear-sky periods under consideration
1141 in our analysis together with the associated standard deviation (vertical bar) together with the
1142 fitted trigonometric function based on 2 sine functions (red). (Center) The 2 sine functions
1143 fitting the hourly time evolution of the BSRN mean surface albedo. (Bottom) Hourly time
1144 evolution (UTC, hour) of the albedo residuals (BSRN fit) and associated Root Mean Square
1145 Error (RMSE), Coefficient of determination (R^2), and Mean Absolute Error (MAE).
1146

← - - - Mis en forme : Interligne : Double



1147
 1148 **Figure 14:** Same as Figure 11 with the albedo inserted in the lowermost panel. Net SR, SWU
 1149 SR, and albedo including the sastrugi effect for ERA5 (red solid line) and CERES (green solid
 1150 line) have also been added in the Figures.
 1151



1152

1153 **Figure 15:** Hourly time evolution (UTC, hour) of the surface albedo observed by the BSRN
 1154 instruments (blue), and using the fit function based on 2 sine functions (red) for the whole
 1155 BSRN data set covering the month of December in 2018, 2019, 2020 and 2021.

1156

← -- Mis en forme : Gauche

Page 12 : [1] Mis en forme	RICAUD Philippe	06/11/2023 11:08:00
Surlignage		
Page 12 : [1] Mis en forme	RICAUD Philippe	06/11/2023 11:08:00
Surlignage		
Page 12 : [1] Mis en forme	RICAUD Philippe	06/11/2023 11:08:00
Surlignage		
Page 12 : [1] Mis en forme	RICAUD Philippe	06/11/2023 11:08:00
Surlignage		
Page 12 : [1] Mis en forme	RICAUD Philippe	06/11/2023 11:08:00
Surlignage		
Page 12 : [1] Mis en forme	RICAUD Philippe	06/11/2023 11:08:00
Surlignage		
Page 12 : [1] Mis en forme	RICAUD Philippe	06/11/2023 11:08:00
Surlignage		
Page 12 : [1] Mis en forme	RICAUD Philippe	06/11/2023 11:08:00
Surlignage		
Page 12 : [1] Mis en forme	RICAUD Philippe	06/11/2023 11:08:00
Surlignage		
Page 12 : [1] Mis en forme	RICAUD Philippe	06/11/2023 11:08:00
Surlignage		
Page 12 : [1] Mis en forme	RICAUD Philippe	06/11/2023 11:08:00
Surlignage		
Page 12 : [2] Mis en forme	RICAUD Philippe	06/11/2023 11:08:00
Surlignage		
Page 12 : [2] Mis en forme	RICAUD Philippe	06/11/2023 11:08:00
Surlignage		
Page 12 : [2] Mis en forme	RICAUD Philippe	06/11/2023 11:08:00
Surlignage		
Page 12 : [2] Mis en forme	RICAUD Philippe	06/11/2023 11:08:00
Surlignage		
Page 12 : [3] Mis en forme	RICAUD Philippe	06/11/2023 11:08:00
Surlignage		
Page 12 : [3] Mis en forme	RICAUD Philippe	06/11/2023 11:08:00
Surlignage		
Page 12 : [3] Mis en forme	RICAUD Philippe	06/11/2023 11:08:00
Surlignage		
Page 12 : [4] Mis en forme	RICAUD Philippe	06/11/2023 11:08:00

Surlignage

Page 12 : [4] Mis en forme	RICAUD Philippe	06/11/2023 11:08:00
-----------------------------------	-----------------	---------------------

Surlignage

Page 12 : [4] Mis en forme	RICAUD Philippe	06/11/2023 11:08:00
-----------------------------------	-----------------	---------------------

Surlignage

Page 12 : [4] Mis en forme	RICAUD Philippe	06/11/2023 11:08:00
-----------------------------------	-----------------	---------------------

Surlignage

Page 12 : [4] Mis en forme	RICAUD Philippe	06/11/2023 11:08:00
-----------------------------------	-----------------	---------------------

Surlignage

Page 12 : [4] Mis en forme	RICAUD Philippe	06/11/2023 11:08:00
-----------------------------------	-----------------	---------------------

Surlignage

Page 12 : [4] Mis en forme	RICAUD Philippe	06/11/2023 11:08:00
-----------------------------------	-----------------	---------------------

Surlignage

Page 12 : [4] Mis en forme	RICAUD Philippe	06/11/2023 11:08:00
-----------------------------------	-----------------	---------------------

Surlignage

Page 12 : [4] Mis en forme	RICAUD Philippe	06/11/2023 11:08:00
-----------------------------------	-----------------	---------------------

Surlignage

Page 12 : [4] Mis en forme	RICAUD Philippe	06/11/2023 11:08:00
-----------------------------------	-----------------	---------------------

Surlignage

Page 12 : [5] Mis en forme	RICAUD Philippe	06/11/2023 11:08:00
-----------------------------------	-----------------	---------------------

Surlignage

Page 12 : [5] Mis en forme	RICAUD Philippe	06/11/2023 11:08:00
-----------------------------------	-----------------	---------------------

Surlignage

Page 12 : [5] Mis en forme	RICAUD Philippe	06/11/2023 11:08:00
-----------------------------------	-----------------	---------------------

Surlignage

Page 12 : [5] Mis en forme	RICAUD Philippe	06/11/2023 11:08:00
-----------------------------------	-----------------	---------------------

Surlignage

Page 12 : [6] Mis en forme	RICAUD Philippe	06/11/2023 11:08:00
-----------------------------------	-----------------	---------------------

Surlignage

Page 12 : [6] Mis en forme	RICAUD Philippe	06/11/2023 11:08:00
-----------------------------------	-----------------	---------------------

Surlignage

Page 12 : [6] Mis en forme	RICAUD Philippe	06/11/2023 11:08:00
-----------------------------------	-----------------	---------------------

Surlignage

Page 12 : [6] Mis en forme	RICAUD Philippe	06/11/2023 11:08:00
-----------------------------------	-----------------	---------------------

Surlignage

Page 12 : [7] Mis en forme	RICAUD Philippe	06/11/2023 11:08:00
-----------------------------------	-----------------	---------------------

Surlignage

Page 12 : [7] Mis en forme	RICAUD Philippe	06/11/2023 11:08:00
-----------------------------------	-----------------	---------------------

Surlignage

Page 12 : [7] Mis en forme	RICAUD Philippe	06/11/2023 11:08:00
-----------------------------------	-----------------	---------------------

Surlignage

Surlignage

Page 12 : [9] Mis en forme	RICAUD Philippe	06/11/2023 11:51:00
-----------------------------------	-----------------	---------------------

Surlignage

Page 12 : [9] Mis en forme	RICAUD Philippe	06/11/2023 11:51:00
-----------------------------------	-----------------	---------------------

Surlignage

Page 12 : [9] Mis en forme	RICAUD Philippe	06/11/2023 11:51:00
-----------------------------------	-----------------	---------------------

Surlignage

Page 12 : [9] Mis en forme	RICAUD Philippe	06/11/2023 11:51:00
-----------------------------------	-----------------	---------------------

Surlignage

Page 12 : [10] Mis en forme	RICAUD Philippe	06/11/2023 11:51:00
------------------------------------	-----------------	---------------------

Surlignage

Page 12 : [10] Mis en forme	RICAUD Philippe	06/11/2023 11:51:00
------------------------------------	-----------------	---------------------

Surlignage

Page 12 : [10] Mis en forme	RICAUD Philippe	06/11/2023 11:51:00
------------------------------------	-----------------	---------------------

Surlignage

Page 12 : [10] Mis en forme	RICAUD Philippe	06/11/2023 11:51:00
------------------------------------	-----------------	---------------------

Surlignage

Page 12 : [10] Mis en forme	RICAUD Philippe	06/11/2023 11:51:00
------------------------------------	-----------------	---------------------

Surlignage

Page 12 : [10] Mis en forme	RICAUD Philippe	06/11/2023 11:51:00
------------------------------------	-----------------	---------------------

Surlignage

Page 12 : [10] Mis en forme	RICAUD Philippe	06/11/2023 11:51:00
------------------------------------	-----------------	---------------------

Surlignage

Page 12 : [10] Mis en forme	RICAUD Philippe	06/11/2023 11:51:00
------------------------------------	-----------------	---------------------

Surlignage

Page 12 : [10] Mis en forme	RICAUD Philippe	06/11/2023 11:51:00
------------------------------------	-----------------	---------------------

Surlignage

Page 12 : [11] Mis en forme	RICAUD Philippe	06/11/2023 11:08:00
------------------------------------	-----------------	---------------------

Surlignage

Page 12 : [11] Mis en forme	RICAUD Philippe	06/11/2023 11:08:00
------------------------------------	-----------------	---------------------

Surlignage

Page 12 : [11] Mis en forme	RICAUD Philippe	06/11/2023 11:08:00
------------------------------------	-----------------	---------------------

Surlignage

Page 12 : [11] Mis en forme	RICAUD Philippe	06/11/2023 11:08:00
------------------------------------	-----------------	---------------------

Surlignage

Page 12 : [12] Mis en forme	RICAUD Philippe	06/11/2023 11:08:00
------------------------------------	-----------------	---------------------

Surlignage

Page 12 : [12] Mis en forme	RICAUD Philippe	06/11/2023 11:08:00
------------------------------------	-----------------	---------------------

Surlignage

Page 12 : [12] Mis en forme	RICAUD Philippe	06/11/2023 11:08:00
------------------------------------	-----------------	---------------------

Surlignage

Surlignage

Page 12 : [14] Mis en forme	RICAUD Philippe	07/11/2023 15:10:00
------------------------------------	-----------------	---------------------

Surlignage

Page 12 : [14] Mis en forme	RICAUD Philippe	07/11/2023 15:10:00
------------------------------------	-----------------	---------------------

Surlignage

Page 12 : [14] Mis en forme	RICAUD Philippe	07/11/2023 15:10:00
------------------------------------	-----------------	---------------------

Surlignage

Page 12 : [15] Mis en forme	RICAUD Philippe	06/11/2023 11:08:00
------------------------------------	-----------------	---------------------

Surlignage

Page 12 : [15] Mis en forme	RICAUD Philippe	06/11/2023 11:08:00
------------------------------------	-----------------	---------------------

Surlignage

Page 12 : [15] Mis en forme	RICAUD Philippe	06/11/2023 11:08:00
------------------------------------	-----------------	---------------------

Surlignage

Page 12 : [16] Mis en forme	RICAUD Philippe	06/11/2023 11:08:00
------------------------------------	-----------------	---------------------

Surlignage

Page 12 : [16] Mis en forme	RICAUD Philippe	06/11/2023 11:08:00
------------------------------------	-----------------	---------------------

Surlignage

Page 12 : [16] Mis en forme	RICAUD Philippe	06/11/2023 11:08:00
------------------------------------	-----------------	---------------------

Surlignage

Page 18 : [17] Mis en forme	RICAUD Philippe	06/11/2023 11:10:00
------------------------------------	-----------------	---------------------

Surlignage

Page 18 : [18] Mis en forme	RICAUD Philippe	06/11/2023 11:10:00
------------------------------------	-----------------	---------------------

Surlignage

Page 18 : [19] Mis en forme	RICAUD Philippe	06/11/2023 11:11:00
------------------------------------	-----------------	---------------------

Surlignage

Page 18 : [20] Mis en forme	RICAUD Philippe	06/11/2023 11:11:00
------------------------------------	-----------------	---------------------

Surlignage

Page 18 : [21] Mis en forme	RICAUD Philippe	06/11/2023 11:11:00
------------------------------------	-----------------	---------------------

Surlignage

Page 18 : [22] Mis en forme	RICAUD Philippe	06/11/2023 11:11:00
------------------------------------	-----------------	---------------------

Surlignage

Page 18 : [23] Mis en forme	RICAUD Philippe	06/11/2023 11:11:00
------------------------------------	-----------------	---------------------

Surlignage

Page 18 : [24] Mis en forme	RICAUD Philippe	06/11/2023 11:11:00
------------------------------------	-----------------	---------------------

Surlignage

Page 18 : [25] Mis en forme	RICAUD Philippe	06/11/2023 11:11:00
------------------------------------	-----------------	---------------------

Surlignage

Page 18 : [26] Mis en forme	RICAUD Philippe	06/11/2023 11:11:00
------------------------------------	-----------------	---------------------

Surlignage

Page 18 : [27] Mis en forme	RICAUD Philippe	06/11/2023 11:11:00
------------------------------------	-----------------	---------------------

Surlignage

Page 18 : [28] Mis en forme	RICAUD Philippe	06/11/2023 11:11:00
Surlignage		
Page 18 : [29] Mis en forme	RICAUD Philippe	06/11/2023 11:11:00
Surlignage		
Page 18 : [30] Mis en forme	RICAUD Philippe	06/11/2023 11:11:00
Surlignage		
Page 18 : [31] Mis en forme	RICAUD Philippe	06/11/2023 11:11:00
Surlignage		
Page 18 : [32] Mis en forme	RICAUD Philippe	06/11/2023 11:11:00
Surlignage		
Page 18 : [33] Mis en forme	RICAUD Philippe	06/11/2023 11:11:00
Surlignage		
Page 18 : [34] Mis en forme	RICAUD Philippe	06/11/2023 11:11:00
Surlignage		
Page 18 : [35] Mis en forme	RICAUD Philippe	06/11/2023 11:11:00
Surlignage		
Page 18 : [36] Mis en forme	RICAUD Philippe	06/11/2023 11:11:00
Surlignage		
Page 18 : [37] Mis en forme	RICAUD Philippe	06/11/2023 11:11:00
Surlignage		
Page 18 : [38] Mis en forme	RICAUD Philippe	06/11/2023 11:11:00
Surlignage		
Page 18 : [39] Mis en forme	RICAUD Philippe	06/11/2023 11:11:00
Surlignage		
Page 18 : [40] Mis en forme	RICAUD Philippe	06/11/2023 11:11:00
Surlignage		
Page 18 : [41] Mis en forme	RICAUD Philippe	06/11/2023 11:11:00
Surlignage		
Page 18 : [42] Mis en forme	RICAUD Philippe	06/11/2023 11:11:00
Surlignage		
Page 18 : [43] Mis en forme	RICAUD Philippe	06/11/2023 11:11:00
Surlignage		
Page 18 : [44] Mis en forme	RICAUD Philippe	06/11/2023 11:11:00
Surlignage		
Page 18 : [45] Mis en forme	RICAUD Philippe	06/11/2023 11:11:00
Surlignage		
Page 18 : [46] Mis en forme	RICAUD Philippe	06/11/2023 11:11:00
Surlignage		
Page 18 : [47] Mis en forme	RICAUD Philippe	06/11/2023 11:11:00
Surlignage		
Page 18 : [48] Mis en forme	RICAUD Philippe	06/11/2023 11:11:00

Surlignage

Page 18 : [49] Mis en forme	RICAUD Philippe	06/11/2023 11:11:00
------------------------------------	-----------------	---------------------

Surlignage

Page 18 : [50] Mis en forme	RICAUD Philippe	06/11/2023 11:11:00
------------------------------------	-----------------	---------------------

Surlignage

Page 18 : [51] Mis en forme	RICAUD Philippe	06/11/2023 11:11:00
------------------------------------	-----------------	---------------------

Surlignage

Page 18 : [52] Mis en forme	RICAUD Philippe	06/11/2023 11:11:00
------------------------------------	-----------------	---------------------

Surlignage

Page 18 : [53] Mis en forme	RICAUD Philippe	06/11/2023 11:11:00
------------------------------------	-----------------	---------------------

Surlignage

Page 18 : [54] Mis en forme	RICAUD Philippe	06/11/2023 11:11:00
------------------------------------	-----------------	---------------------

Surlignage

Page 18 : [55] Mis en forme	RICAUD Philippe	06/11/2023 11:11:00
------------------------------------	-----------------	---------------------

Surlignage

Page 18 : [56] Mis en forme	RICAUD Philippe	06/11/2023 11:11:00
------------------------------------	-----------------	---------------------

Surlignage

Page 18 : [57] Mis en forme	RICAUD Philippe	06/11/2023 11:12:00
------------------------------------	-----------------	---------------------

Surlignage

Page 18 : [58] Mis en forme	RICAUD Philippe	06/11/2023 11:12:00
------------------------------------	-----------------	---------------------

Surlignage

Page 18 : [59] Mis en forme	RICAUD Philippe	06/11/2023 11:12:00
------------------------------------	-----------------	---------------------

Surlignage

Page 18 : [60] Mis en forme	RICAUD Philippe	06/11/2023 11:12:00
------------------------------------	-----------------	---------------------

Surlignage

Page 18 : [61] Mis en forme	RICAUD Philippe	06/11/2023 11:12:00
------------------------------------	-----------------	---------------------

Surlignage

Page 18 : [62] Mis en forme	RICAUD Philippe	06/11/2023 11:12:00
------------------------------------	-----------------	---------------------

Surlignage

Page 18 : [63] Mis en forme	RICAUD Philippe	07/11/2023 15:21:00
------------------------------------	-----------------	---------------------

Surlignage

Page 18 : [64] Mis en forme	RICAUD Philippe	06/11/2023 11:12:00
------------------------------------	-----------------	---------------------

Surlignage

Page 18 : [65] Mis en forme	RICAUD Philippe	06/11/2023 11:12:00
------------------------------------	-----------------	---------------------

Surlignage

Page 18 : [66] Mis en forme	RICAUD Philippe	06/11/2023 11:12:00
------------------------------------	-----------------	---------------------

Surlignage

Page 19 : [67] Mis en forme	RICAUD Philippe	06/11/2023 11:12:00
------------------------------------	-----------------	---------------------

Surlignage

Page 19 : [67] Mis en forme	RICAUD Philippe	06/11/2023 11:12:00
------------------------------------	-----------------	---------------------

Surlignage

Page 19 : [67] Mis en forme	RICAUD Philippe	06/11/2023 11:12:00
Surlignage		
Page 19 : [67] Mis en forme	RICAUD Philippe	06/11/2023 11:12:00
Surlignage		
Page 19 : [67] Mis en forme	RICAUD Philippe	06/11/2023 11:12:00
Surlignage		
Page 19 : [68] Mis en forme	RICAUD Philippe	06/11/2023 11:12:00
Surlignage		
Page 19 : [68] Mis en forme	RICAUD Philippe	06/11/2023 11:12:00
Surlignage		
Page 19 : [68] Mis en forme	RICAUD Philippe	06/11/2023 11:12:00
Surlignage		
Page 19 : [68] Mis en forme	RICAUD Philippe	06/11/2023 11:12:00
Surlignage		
Page 19 : [69] Mis en forme	RICAUD Philippe	06/11/2023 11:12:00
Surlignage		
Page 19 : [69] Mis en forme	RICAUD Philippe	06/11/2023 11:13:00
Surlignage		
Page 19 : [70] Mis en forme	RICAUD Philippe	06/11/2023 11:13:00
Surlignage		
Page 19 : [70] Mis en forme	RICAUD Philippe	06/11/2023 11:13:00
Surlignage		
Page 19 : [70] Mis en forme	RICAUD Philippe	06/11/2023 11:13:00
Surlignage		
Page 19 : [70] Mis en forme	RICAUD Philippe	06/11/2023 11:13:00
Surlignage		
Page 19 : [70] Mis en forme	RICAUD Philippe	06/11/2023 11:13:00
Surlignage		
Page 19 : [70] Mis en forme	RICAUD Philippe	06/11/2023 11:13:00
Surlignage		
Page 19 : [71] Mis en forme	RICAUD Philippe	06/11/2023 11:13:00
Surlignage		
Page 19 : [71] Mis en forme	RICAUD Philippe	06/11/2023 11:13:00
Surlignage		
Page 19 : [71] Mis en forme	RICAUD Philippe	06/11/2023 11:13:00
Surlignage		
Page 19 : [71] Mis en forme	RICAUD Philippe	06/11/2023 11:13:00
Surlignage		
Page 19 : [71] Mis en forme	RICAUD Philippe	06/11/2023 11:13:00
Surlignage		
Page 19 : [72] Mis en forme	RICAUD Philippe	06/11/2023 11:13:00

Surlignage

Page 19 : [72] Mis en forme	RICAUD Philippe	06/11/2023 11:13:00
------------------------------------	------------------------	----------------------------

Surlignage

Page 19 : [72] Mis en forme	RICAUD Philippe	06/11/2023 11:13:00
------------------------------------	------------------------	----------------------------

Surlignage

Page 19 : [72] Mis en forme	RICAUD Philippe	06/11/2023 11:13:00
------------------------------------	------------------------	----------------------------

Surlignage

Page 19 : [72] Mis en forme	RICAUD Philippe	06/11/2023 11:13:00
------------------------------------	------------------------	----------------------------

Surlignage

Page 19 : [72] Mis en forme	RICAUD Philippe	06/11/2023 11:13:00
------------------------------------	------------------------	----------------------------

Surlignage

Page 19 : [73] Mis en forme	RICAUD Philippe	06/11/2023 11:13:00
------------------------------------	------------------------	----------------------------

Surlignage

Page 19 : [73] Mis en forme	RICAUD Philippe	06/11/2023 11:13:00
------------------------------------	------------------------	----------------------------

Surlignage

Page 19 : [73] Mis en forme	RICAUD Philippe	06/11/2023 11:13:00
------------------------------------	------------------------	----------------------------

Surlignage

Page 19 : [73] Mis en forme	RICAUD Philippe	06/11/2023 11:13:00
------------------------------------	------------------------	----------------------------

Surlignage

Page 19 : [73] Mis en forme	RICAUD Philippe	06/11/2023 11:13:00
------------------------------------	------------------------	----------------------------

Surlignage

Page 19 : [74] Mis en forme	RICAUD Philippe	06/11/2023 11:13:00
------------------------------------	------------------------	----------------------------

Surlignage

Page 19 : [74] Mis en forme	RICAUD Philippe	06/11/2023 11:13:00
------------------------------------	------------------------	----------------------------

Surlignage

Page 19 : [74] Mis en forme	RICAUD Philippe	06/11/2023 11:13:00
------------------------------------	------------------------	----------------------------

Surlignage

Page 19 : [74] Mis en forme	RICAUD Philippe	06/11/2023 11:13:00
------------------------------------	------------------------	----------------------------

Surlignage

Page 19 : [74] Mis en forme	RICAUD Philippe	06/11/2023 11:13:00
------------------------------------	------------------------	----------------------------

Surlignage

Page 19 : [74] Mis en forme	RICAUD Philippe	06/11/2023 11:13:00
------------------------------------	------------------------	----------------------------

Surlignage

Page 19 : [74] Mis en forme	RICAUD Philippe	06/11/2023 11:13:00
------------------------------------	------------------------	----------------------------

Surlignage

Page 19 : [74] Mis en forme	RICAUD Philippe	06/11/2023 11:13:00
------------------------------------	------------------------	----------------------------

Surlignage

Page 19 : [74] Mis en forme	RICAUD Philippe	06/11/2023 11:13:00
------------------------------------	------------------------	----------------------------

Surlignage

Page 19 : [75] Mis en forme	RICAUD Philippe	06/11/2023 11:13:00
------------------------------------	------------------------	----------------------------

Exposant, Surlignage

Page 19 : [75] Mis en forme	RICAUD Philippe	06/11/2023 11:13:00
Exposant, Surlignage		
Page 19 : [75] Mis en forme	RICAUD Philippe	06/11/2023 11:13:00
Exposant, Surlignage		
Page 19 : [75] Mis en forme	RICAUD Philippe	06/11/2023 11:13:00
Exposant, Surlignage		
Page 19 : [75] Mis en forme	RICAUD Philippe	06/11/2023 11:13:00
Exposant, Surlignage		
Page 19 : [76] Mis en forme	RICAUD Philippe	06/11/2023 11:13:00
Surlignage		
Page 19 : [76] Mis en forme	RICAUD Philippe	06/11/2023 11:13:00
Surlignage		
Page 19 : [76] Mis en forme	RICAUD Philippe	06/11/2023 11:13:00
Surlignage		
Page 19 : [76] Mis en forme	RICAUD Philippe	06/11/2023 11:13:00
Surlignage		
Page 19 : [76] Mis en forme	RICAUD Philippe	06/11/2023 11:13:00
Surlignage		
Page 19 : [76] Mis en forme	RICAUD Philippe	06/11/2023 11:13:00
Surlignage		
Page 30 : [77] Mis en forme	RICAUD Philippe	06/11/2023 11:15:00
Surlignage		
Page 30 : [77] Mis en forme	RICAUD Philippe	06/11/2023 11:15:00
Surlignage		
Page 30 : [77] Mis en forme	RICAUD Philippe	06/11/2023 11:15:00
Surlignage		
Page 30 : [78] Mis en forme	RICAUD Philippe	06/11/2023 11:15:00
Surlignage		
Page 30 : [78] Mis en forme	RICAUD Philippe	06/11/2023 11:15:00
Surlignage		
Page 30 : [78] Mis en forme	RICAUD Philippe	06/11/2023 11:15:00
Surlignage		
Page 30 : [79] Mis en forme	RICAUD Philippe	06/11/2023 11:15:00
Surlignage		
Page 30 : [79] Mis en forme	RICAUD Philippe	06/11/2023 11:15:00
Surlignage		
Page 30 : [79] Mis en forme	RICAUD Philippe	06/11/2023 11:15:00

Surlignage

Page 30 : [79] Mis en forme	RICAUD Philippe	06/11/2023 11:15:00
------------------------------------	-----------------	---------------------

Surlignage

Page 30 : [79] Mis en forme	RICAUD Philippe	06/11/2023 11:15:00
------------------------------------	-----------------	---------------------

Surlignage

Page 30 : [79] Mis en forme	RICAUD Philippe	06/11/2023 11:15:00
------------------------------------	-----------------	---------------------

Surlignage

Page 30 : [80] Mis en forme	RICAUD Philippe	06/11/2023 11:15:00
------------------------------------	-----------------	---------------------

Surlignage

Page 30 : [80] Mis en forme	RICAUD Philippe	06/11/2023 11:15:00
------------------------------------	-----------------	---------------------

Surlignage

Page 30 : [80] Mis en forme	RICAUD Philippe	06/11/2023 11:15:00
------------------------------------	-----------------	---------------------

Surlignage

Page 30 : [80] Mis en forme	RICAUD Philippe	06/11/2023 11:15:00
------------------------------------	-----------------	---------------------

Surlignage

Page 30 : [80] Mis en forme	RICAUD Philippe	06/11/2023 11:15:00
------------------------------------	-----------------	---------------------

Surlignage

Page 30 : [80] Mis en forme	RICAUD Philippe	06/11/2023 11:15:00
------------------------------------	-----------------	---------------------

Surlignage

Page 30 : [80] Mis en forme	RICAUD Philippe	06/11/2023 11:15:00
------------------------------------	-----------------	---------------------

Surlignage

Page 30 : [80] Mis en forme	RICAUD Philippe	06/11/2023 11:15:00
------------------------------------	-----------------	---------------------

Surlignage

Page 30 : [80] Mis en forme	RICAUD Philippe	06/11/2023 11:15:00
------------------------------------	-----------------	---------------------

Surlignage

Page 30 : [80] Mis en forme	RICAUD Philippe	06/11/2023 11:15:00
------------------------------------	-----------------	---------------------

Surlignage

Page 30 : [80] Mis en forme	RICAUD Philippe	06/11/2023 11:15:00
------------------------------------	-----------------	---------------------

Surlignage

Page 30 : [80] Mis en forme	RICAUD Philippe	06/11/2023 11:15:00
------------------------------------	-----------------	---------------------

Surlignage

Page 30 : [80] Mis en forme	RICAUD Philippe	06/11/2023 11:15:00
------------------------------------	-----------------	---------------------

Surlignage

Page 30 : [81] Mis en forme	RICAUD Philippe	06/11/2023 11:16:00
------------------------------------	-----------------	---------------------

Surlignage

Page 30 : [81] Mis en forme	RICAUD Philippe	06/11/2023 11:16:00
------------------------------------	-----------------	---------------------

Surlignage

Page 30 : [81] Mis en forme	RICAUD Philippe	06/11/2023 11:16:00
------------------------------------	-----------------	---------------------

Surlignage

Page 30 : [81] Mis en forme	RICAUD Philippe	06/11/2023 11:16:00
------------------------------------	-----------------	---------------------

Surlignage

Surlignage

Page 30 : [83] Mis en forme

RICAUD Philippe

06/11/2023 11:16:00

Surlignage